952217

68-

N.L.

First Quarterly Progress Report

THERMIONIC RESEARCH AND DEVELOPMENT PROGRAM

Prepared for
Jet Propulsion Laboratory
California Institute of Technology
4800 Oak Grove Drive
Pasadena, California
Attention: J. M. Skipton

Contract 952217

EOS Report 4006-Q-1 12 July 1968

ELECTRO-OPTICAL SYSTEMS, INC.
A XEROX COMPANY
PASADENA, CALIFORNIA 91107 • 213/351-2351

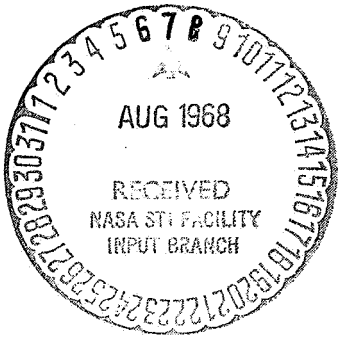

First Quarterly Progress Report

THERMIONIC RESEARCH AND DEVELOPMENT PROGRAM

Prepared for
Jet Propulsion Laboratory
California Institute of Technology
4800 Oak Grove Drive
Pasadena, California
Attention: J. M. Skipton

Contract 952217

EOS Report 4006-Q-1 12 July 1968

Prepared by
D. L. Jacobson
R. Hamerdinger
A. Campbell

Approved by

A. O. Jensen, Manager
Electro-Optical and Solid State Technology Division

ELECTRO-OPTICAL SYSTEMS, INC.
A XEROX COMPANY

CONTENTS

ILLUSTRATIONS

SECTION 1

INTRODUCTION

The progress described in this, the first quarterly report, is being performed under JPL Contract 952217, a 12-month, three-task program of advanced thermionic converter development.

The first task consists of an investigation of single crystal rhenium electrodes or other refractory materials for the purpose of yielding a low work function collector surface. Specific investigations include vacuum emission vehicle determination of the effective and Richardson work functions as well as qualitative and quantitative examination of electrode surfaces using a thermionic emission microscope. Metallurgical examinations include X ray diffraction and metallographic and spectrographic analyses. These same electrodes will then be investigated in a variable parameter test vehicle for minimum work function and optimized power output. Based upon variable parameter test vehicle data, a planar converter will be fabricated and tested for the purpose of comparing test vehicle to converter performance.

Task II consists of the investigation of vapor-deposited tungsten-20 percent rhenium alloy electrodes in the same manner as in Task I, i.e., utilizing vacuum emission, electron emission microscope, and variable parameter vehicle evaluations with, however, the subsequent fabrication and testing of two planar converters.

Task III completes the program effort with the design, fabrication, and test of cylindrical thermionic converters for the principal purpose of providing a direct performance comparison between planar and cylindrical converters.

SECTION 2

ELECTRODE MATERIALS EVALUATION (TASK I)

Two special purpose devices previously designed and built by EOS for electrode material evaluation are being utilized in Task I investigations. The first device, a vacuum emission vehicle, is employed to measure the average effective bare work function of candidate electrode materials. The second device, the EOS thermionic emission microscope, contains a Faraday cage for the measurement of the effective work function of individual grains and a phosphor screen for displaying the fine grain structure for visual observation and subsequent emission micrograph documentation. The average value of a large number of individual Faraday cage measurements then provides a comparison to the average measurement from the vacuum emission vehicle. Electron emission scans of the electrode surface are also constructed for investigation of effective work function variations within single grains and across grain boundaries.

For Task I, the emission microscope was modified to operate at a magnification of approximately 80X to accommodate the relatively large grains of the single crystal rhenium and (110) single crystal molybdenum electrodes. The modification procedure involved the removal of the projection lens, thus shortening the distance from the immersion lens to the phosphor screen and reducing the magnification. The decelerating collector/Faraday cage assembly was relocated in another part of the microscope to accommodate the phosphor screen placement. Figure 2-1 is a schematic of the present modified emission microscope with voltage ranges indicated.

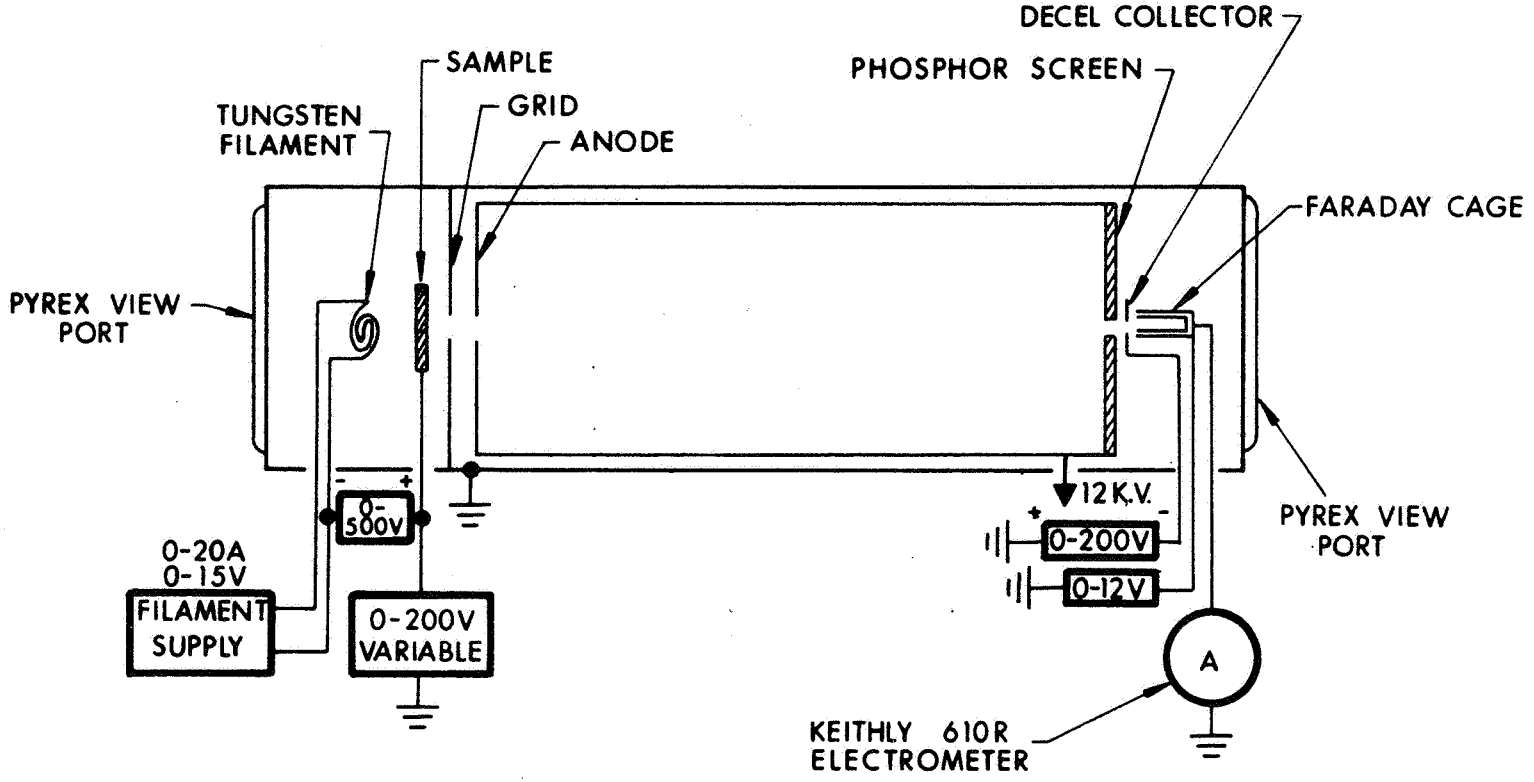

Figure 2-1. Thermionic Emission Microscope Schematic

2.1 (110) SINGLE CRYSTAL MOLYBDENUM

2.1.1 ELECTRON EMISSION MICROSCOPE INVESTIGATION OF (110) MOLYBDENUM

Single crystal molybdenum with the (110) crystal plane oriented parallel to the surface was chosen for investigation in the modified electron emission microscope.

The effective work function of (110) molybdenum was determined by individual Faraday cage measurements and by scanning techniques. The difference in work function across low angle grain boundaries was also determined. A rough estimate of the effect of recrystallized grains of scribe lines upon the overall effective work function was made. The primary objective of the emission microscope measurements is to provide a comparison of effective work function with vacuum emission vehicle measurements and other techniques referenced from the literature.

The molybdenum single crystal was electron beam welded onto a molybdenum support structure for mounting in the microscope. The emission surface was fine-polished with Linde alumina A and B, then diamond scribed. Figure 2-2 is a sketch of a portion at the center of the surface. The center square is 0.050 in. per side, and the other scribe lines are 0.025 in. apart. Two wires, exactly 2 in. apart, were spot welded to the back of the phosphor screen holding plate for magnification determination. By choosing a point on a scribe line coincident with one wire and moving it to coincide with the second wire, the magnification could be directly determined by simultaneous readings of verniers on the drive mechanism. The exact magnification, as a result of the previously described modifications, is dependent upon the voltages applied to the grid and anode portion of the lens. The performance of the Faraday cage was characterized by varying the decelerating

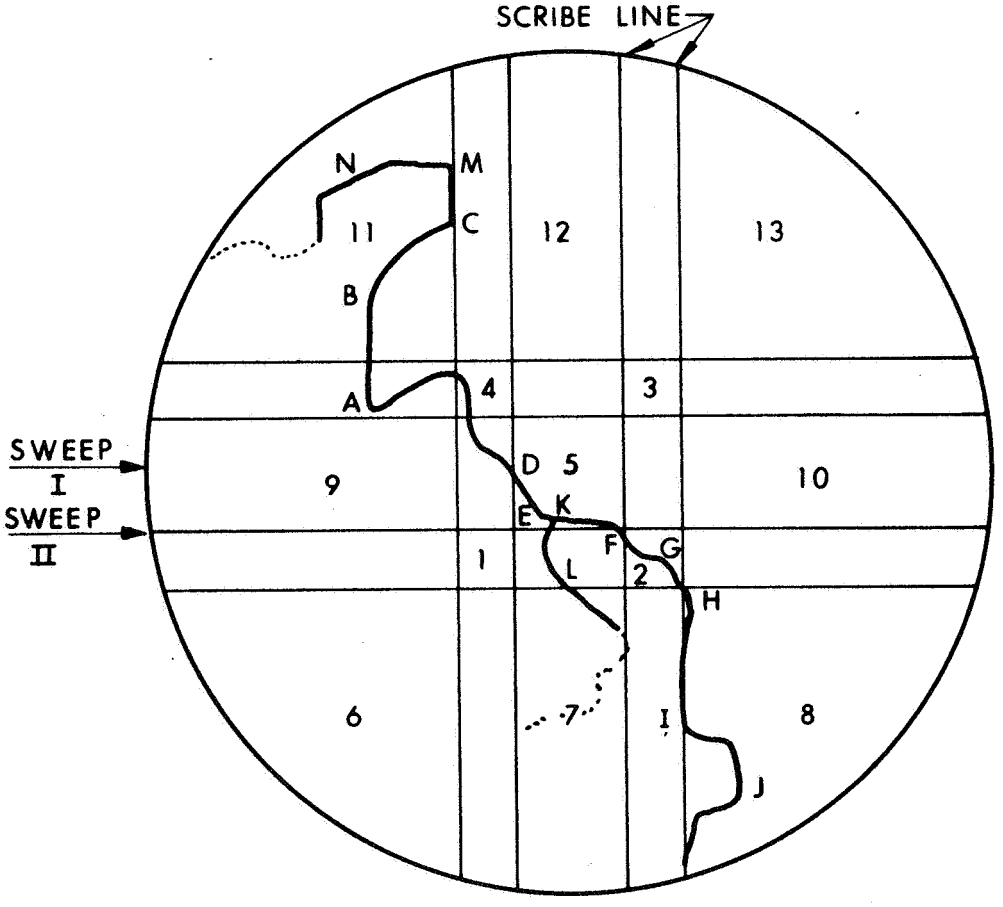

Figure 2-2. Molybdenum Single Crystal (110) Orientation as Seen on Crystal Surface Showing Low Angle Grain Boundary. Magnification 11X

voltage and plotting it as a function of Faraday cage current. The grid voltage was 200 volts and the accelerating voltage was 12,250 volts for the curve shown in Fig. 2-3. It can be seen that in the range of operation of the decelerating grid voltage (i.e., 180 to 220 volts), the Faraday cage current collected is independent of the decelerating voltage.

The second phase of this investigation involved the recrystallization and grain growth of the work-hardened single crystal surface, and the measurement of electron emission with calculated effective work function values for characterizing the (110) single crystal material.

Returning to Fig. 2-2, the irregular line through the sketch of the crystal face approximates the position of a low angle grain boundary. The mapping was accomplished by recording the x-y vernier settings of the drive mechanism as the sample was driven to follow the grain boundary. Scribe line intersections were then used as references in plotting the boundary. The letters refer to points where x-y settings were recorded. The numbers in various areas are for reference for emission micrographs and Faraday cage measurement locations.

Figure 2-4a is an emission micrograph of area #2 on Fig. 2-2 taken with the sample at a temperature of 1564^{o}C. All temperatures reported are true hohlraum temperatures. The sample had been heat treated at 1564^{o}C for three hours. The scribe lines can be seen as consisting of various light grains where recovery and recrystallization have taken place. The dark spot in the middle and continuing to the bottom of the micrograph is the Faraday cage holder. Other white spots away from the scribe lines may be either material pull-out from polishing or thermal etch pits. The low angle grain boundary can be seen by noting the slight difference in background intensity. When comparing the low angle grain boundary in Fig. 2-4a with area #2 shown in Fig. 2-2,

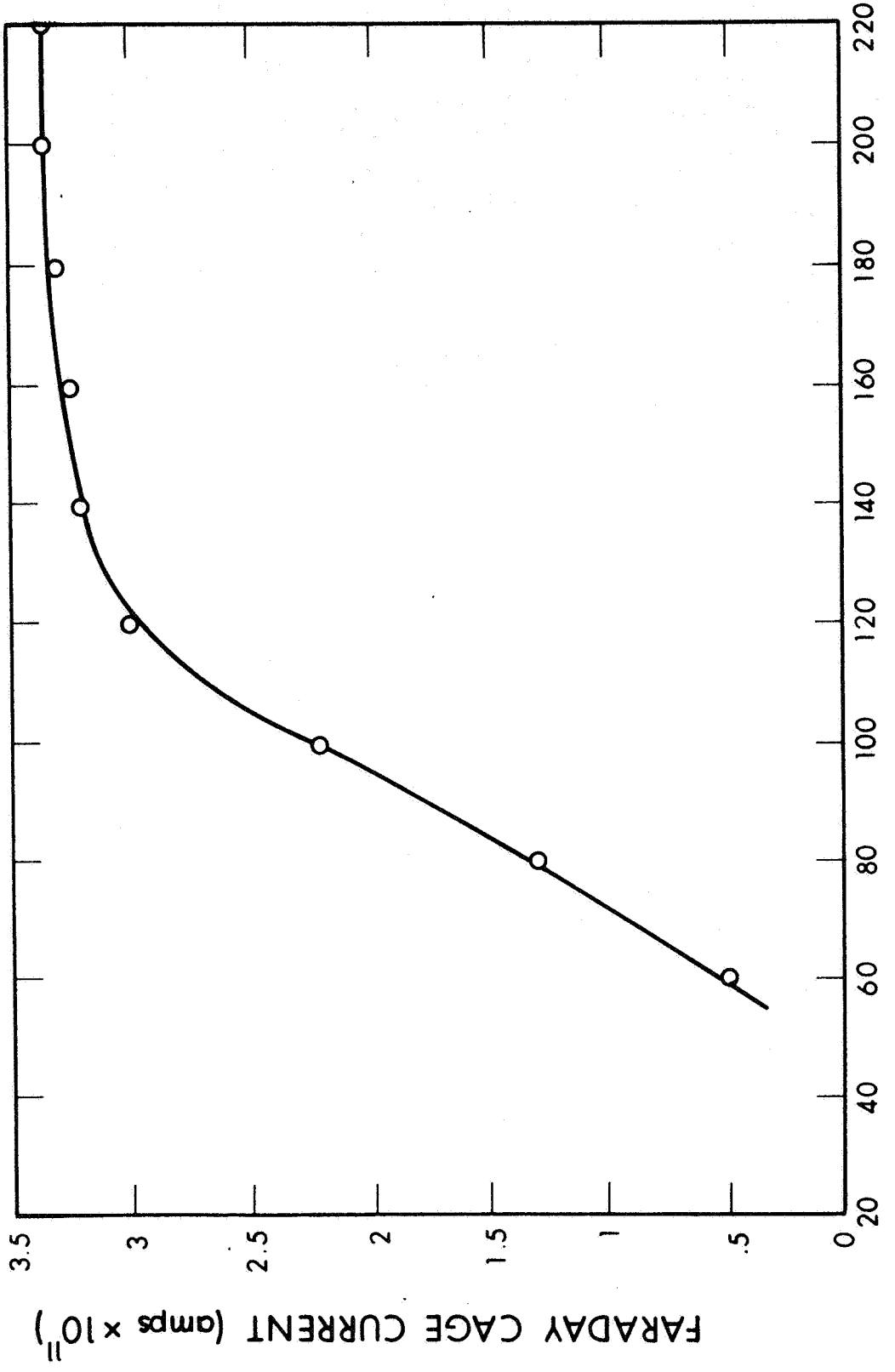

Figure 2-3. Faraday Cage Current versus Accelerating Voltage

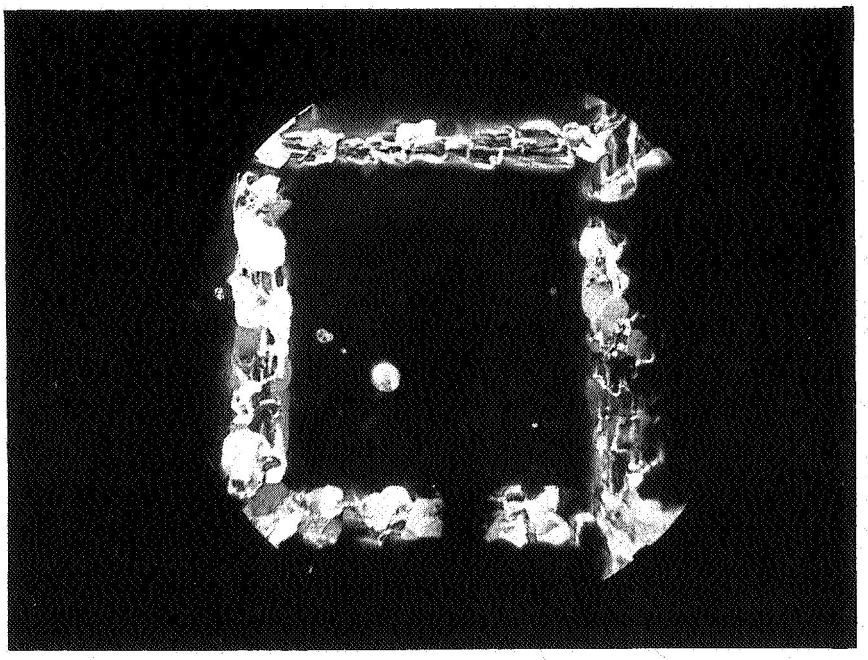

561

a. 1564°C After 3 Hours at 1564°C. Magnified 88X

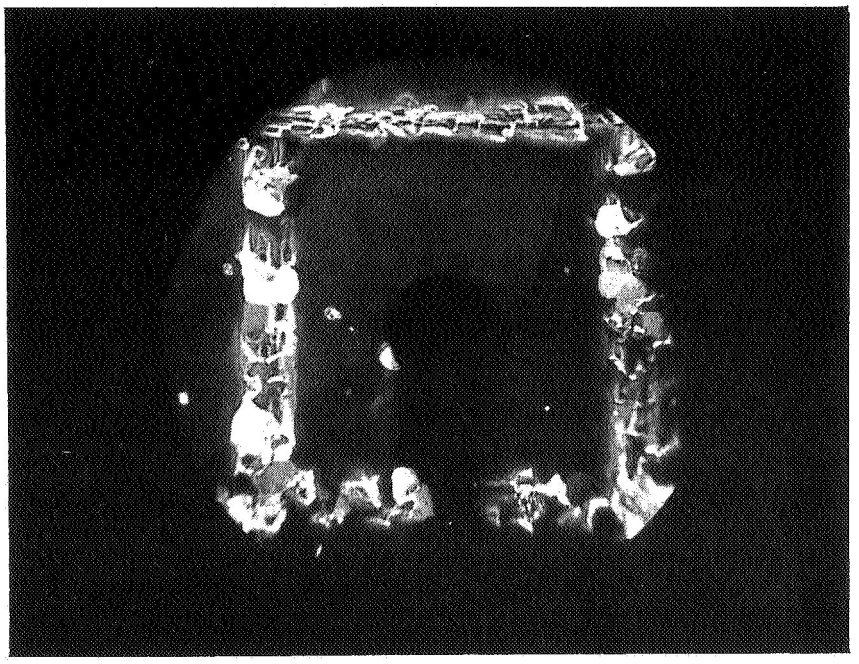

562

b. 1564°C After 8 Hours at 1564°C and 2 Hours at 1717°C. Magnified 84X

Figure 2-4. Electron Emission Micrograph of Molybdenum (110) Single Crystal

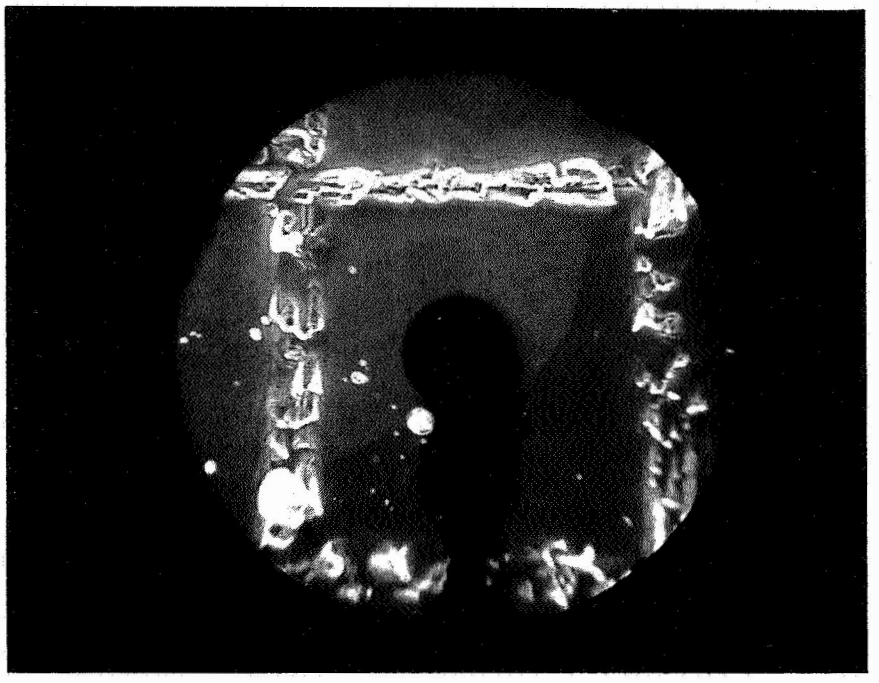

c. 1717°C After 16 Hours at 1564°C, 2.5 Hours at 1717°C, 2.5 Hours at 1768°C, and 1 Hour at 1923°C. Magnified 82X

Figure 2-4. Electron Emission Micrograph of Molybdenum (110) Single Crystal (contd)

the location with respect to the two is inverse, since the image produced on the phosphor screen of the emission microscope is inverted with respect to the actual sample surface. Figure 2-4b is an emission micrograph of area #2 after 8 hours at 1564°C and 2 hours at 1717°C. Figure 2-4c shows the same area after 16 hours at 1564°C, 2-1/2 hours at 1717°C, 2-1/2 hours at 1769°C, and 1 hour at 1923°C. Considerable secondary recrystallization has taken place as the single crystal matrix has grown at the expense of the recrystallized grains due to scribing.

Emission measurements were made of various areas of the sample on either side of the low angle grain boundary and on small grains of the scribe marks. Table I shows individual Faraday cage emission measurements with calculated effective work function values, the temperature of the sample at which they were taken, and the corresponding area referred to Fig. 2-2. The "left" or "right" indicated beside area numbers signifies which side of the low angle grain boundary the measurement was taken.

The work function values calculated in Table I from Faraday cage emission measurements, at a given temperature (i.e., either at 1990°K or at 1837°K) and on the same side of the low angle grain boundary are in every case within experimental error. The area to the left of the low angle grain boundary in Fig. 2-4 appears lighter in the emission micrographs than the area to the right, and this observation is consistent with the emission measurements and effective work function calculations of Table I. The work function of the dark area is in every case (for a given temperature) lower than the adjacent light area. Emission measurements were made in area #2 at 1990°K and in area #5 at 1837°K on each side of the low angle grain boundary with the measured areas in each case being adjacent to one another and less than 0.010 in. from the grain boundary. The difference in work function across the grain boundary in area #2 at 1990°K was 0.07 eV and in area #5 at 1837°K was 0.09 eV.

TABLE I

EFFECTIVE WORK FUNCTION OF THERMIONIC (110) SINGLE CRYSTAL MOLYBDENUM DETERMINED FROM ELECTRON EMISSION MICROSCOPE FARADAY CAGE MEASUREMENTS

Magnification	Sample Temperature (^{o}K)	Area Number	Faraday Cage Current (amps)	ϕ_{eff}(eV)
82X	1990	1 (left)	3.6×10^{-10}	4.82
82X	1990	3 (right)	2.62×10^{-10}	4.90
82X	1990	4 (right)	2.82×10^{-10}	4.88
82X	1990	2 (left)	3.2×10^{-10}	4.85
82X	1990	2 (right)	2.35×10^{-10}	4.92
88X	1837	5 (left)	2.43×10^{-11}	4.84
88X	1837	5 (right)	1.30×10^{-11}	4.94
88X	1897	6 (left)	1.6×10^{-11}	4.91
88X	1837	9 (left)	1.72×10^{-11}	4.90
88X	1837	3 (right)	2.2×10^{-11}	4.86
88X	1837	4 (right)	2.2×10^{-11}	4.86

Figure 2-5 is an electron emission microscope scan across the low angle grain boundary in area #5, as shown in the emission micrograph, Fig. 2-6. The sweep speed was approximately 0.0001 in. per second. The grain boundary appears to be about 0.001 in. from plateau to plateau, but as Fig. 2-6 shows the grain boundary is at a 45^{o} angle to the survey direction (survey direction was from left to right in Fig. 2-6) which would tend to reveal a slightly wider boundary thickness than actually exists. From the scan, the high emission area current is approximately 3×10^{-11} amp, the low emission area 2×10^{-11} amp. Subsequent calculation produces effective work functions of 4.79 eV and 4.88 eV, respectively. These values, when compared with earlier individual Faraday cage emission measurement from each side of the low angle grain boundary in area #5 (see Table I) are within experimental error.

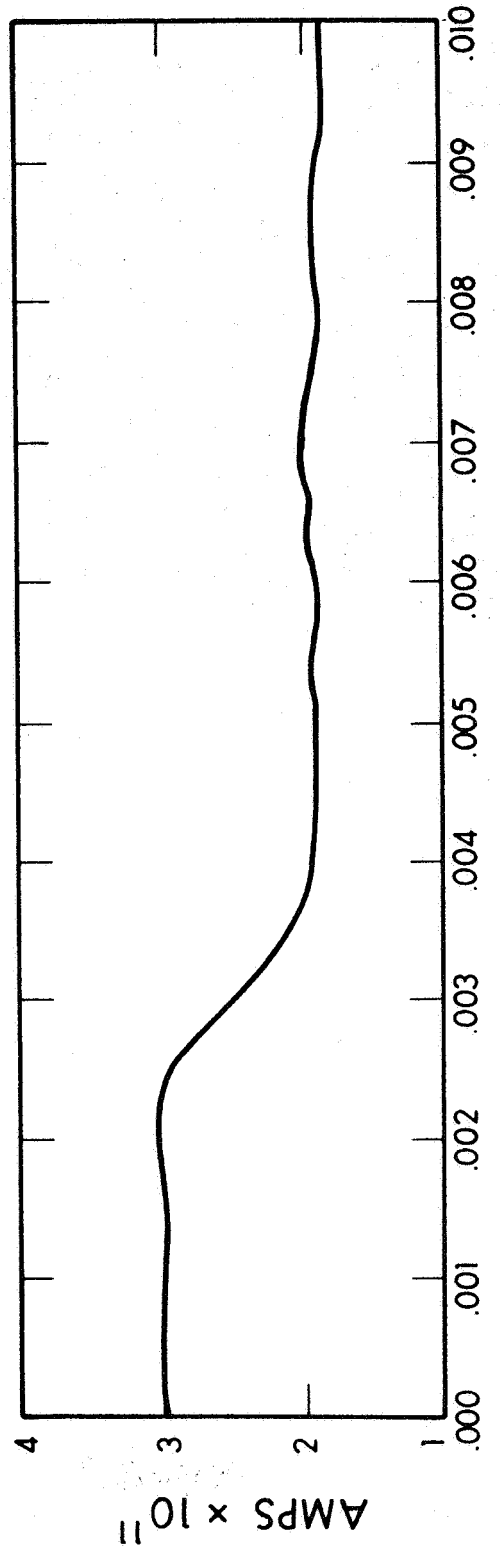

Figure 2-5. Electron Emission Microscope Scan of Low Angle Grain Boundary in (110) Single Crystal Molybdenum. Sample at 1564°C. Scan Across Grain Boundary in Area #5

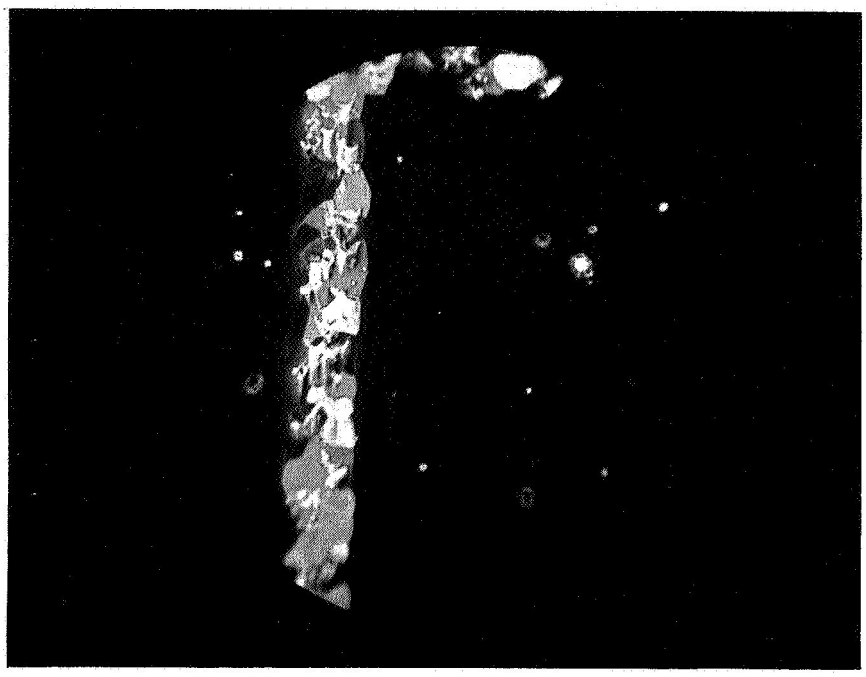

Figure 2-6. Electron Emission Micrograph of (110) Single Crystal Molybdenum Low Angle Grain Boundary at 1564°C After Heat Treating for 8 Hours at 1564°C. Magnification 84X

Figure 2-7 is an electron emission microscope scan from left to right, according to Fig. 2-2, across areas #9, #5, and #10. The scan was taken across the sample where the low angle grain boundary intersects the scribe line (point D as shown in Fig. 2-2). This is also shown in Fig. 2-7, where the average background current drops off after the scan passes through scribe line 2. The spikes not labeled are caused by high emission from material pull-out during polishing or from thermal etch pits. These small areas are also visible on any of the emission micrographs. The scan was taken after heat treating at 1564°C for 18 hours, at 1717°C for 2-1/2 hours, at 1768° for 2-1/2 hours and at 1923°C for 1 hour. The intensity from scribe line 3 is seen to be much less than for the other three scribe lines. This is because secondary recrystallization was nearly complete over the region where the scan was made. The peak currents collected when crossing scribe lines 1, 2, and 4 are not shown in Fig. 2-7 but individual electrometer readings were recorded as follows: (1) 1.0×10^{-10} amp, (2) 2.0×10^{-10} amp, (4) 2.6×10^{-10} amp. The respective calculated effective work functions are: (1) 4.62 eV, (2) 4.53 eV, and (4) 4.48 eV. The approximate average current to the left of the low angle grain boundary is 2.8×10^{-11} amp and to the right it is 1.85×10^{-11} amp. The corresponding effective work functions are 4.83 eV and 4.91 eV, respectively. These values compare favorably with the electron emission scan of Fig. 2-5 across the low angle grain boundary from which effective work functions of 4.79 eV and 4.88 eV were calculated. The difference in the two sets of values is (4.91-4.88) 0.03 eV on the high emission side, thus showing that the work function values from two different scan locations are well within experimental error (±0.04 eV).

Three recent experimental determinations of the work function of (110) molybdenum are listed in Table II. The reported values are Richardson work functions and the A constants are reported here since it was

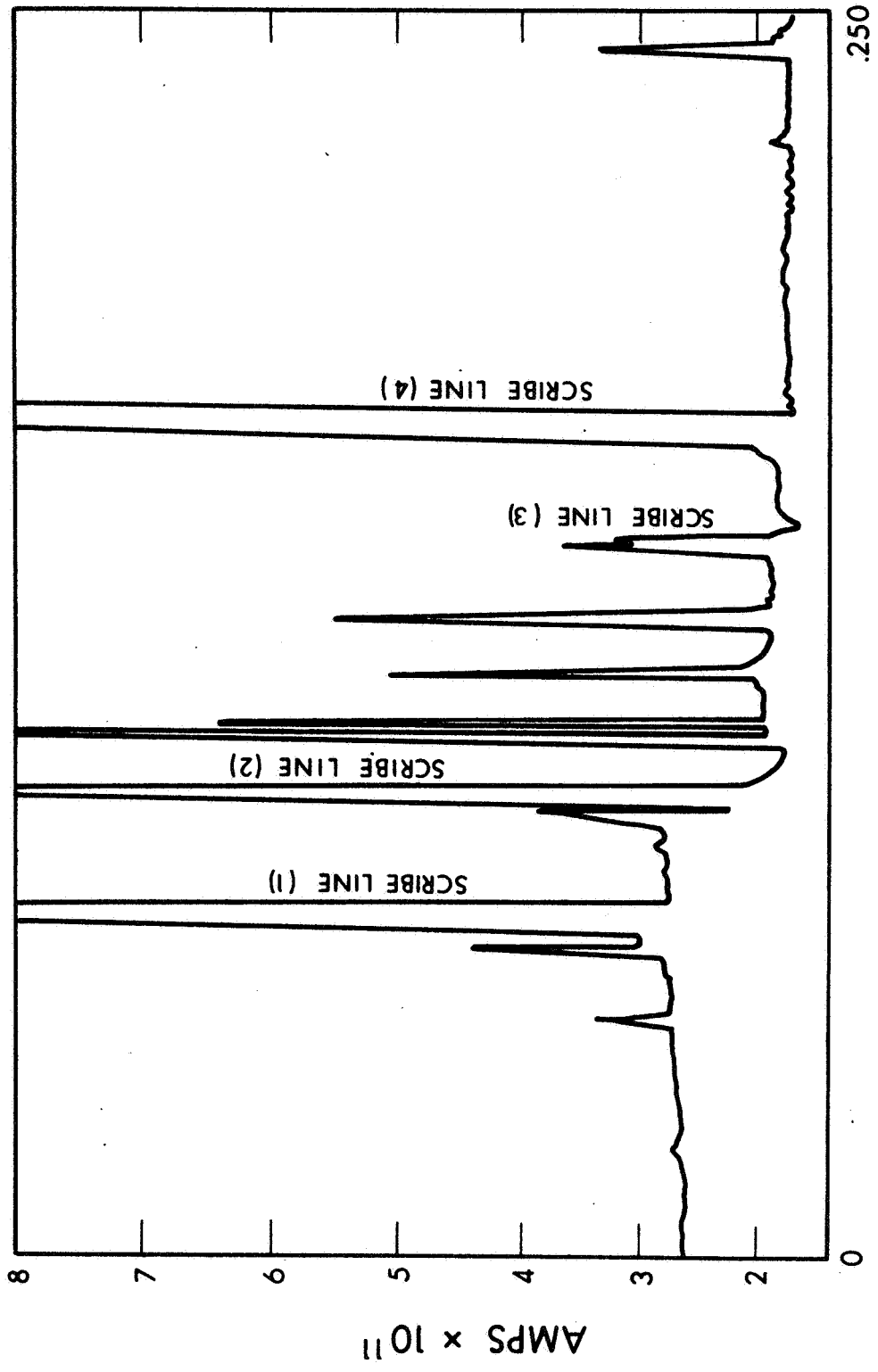

Figure 2-7. Electron Emission Microscope Scan Across Areas 9, 5, and 10 (see Fig. 2-2) of (110) Single Crystal Molybdenum Crystal at 1564°C

necessary to convert the Richardson work functions to effective work functions (A = 120 amps/deg^2-cm^2) to make exact comparisons with the values determined from the electron emission microscope measurements. The temperature ranges over which the Richardson plots were made are also listed with the appropriate work functions in Table II.

TABLE II

WORK FUNCTIONS OF (110) MOLYBDENUM FROM LITERATURE

ϕ Richardson (ev)	A (amps/deg^2-cm^2)	T_e (^{o}K)	Converted ϕ_{eff}(eV)
5.10 ±0.05[1]	270 ±20	(1700^{o}K-2100^{o}K)	4.98 ±0.05
5.00 ±0.05[2]	125 ±15	(1700^{o}K-2000^{o}K)	5.00 ±0.05
4.90 ±0.07[3]	125*	(1600^{o}K-1900^{o}K)	4.90 ±0.07

* Not given in paper.

The effective work function values of Table I can be compared with the effective work function values of Table II. The high work function side of the low angle grain boundary is seen to compare well (within experimental error) with the literature values.

2.1.2 VACUUM EMISSION VEHICLE MEASUREMENTS OF (110) MOLYBDENUM

Upon completion of the electron emission microscope measurements, the same single crystal molybdenum sample was removed from the emission microscope and mounted in the vacuum emission vehicle for average effective work function determinations, the main objective being to provide a comparison with the emission microscope measurements. A second objective was to obtain a rough estimate of the effect of the recrystallized grains of the scribe lines upon the overall effective work function.

Figure 2-8 shows three vacuum emission vehicle Schottky plots with the square root of the applied field, $\sqrt{E}$, versus electron current, I. Interelectrode spacings were determined experimentally at the listed

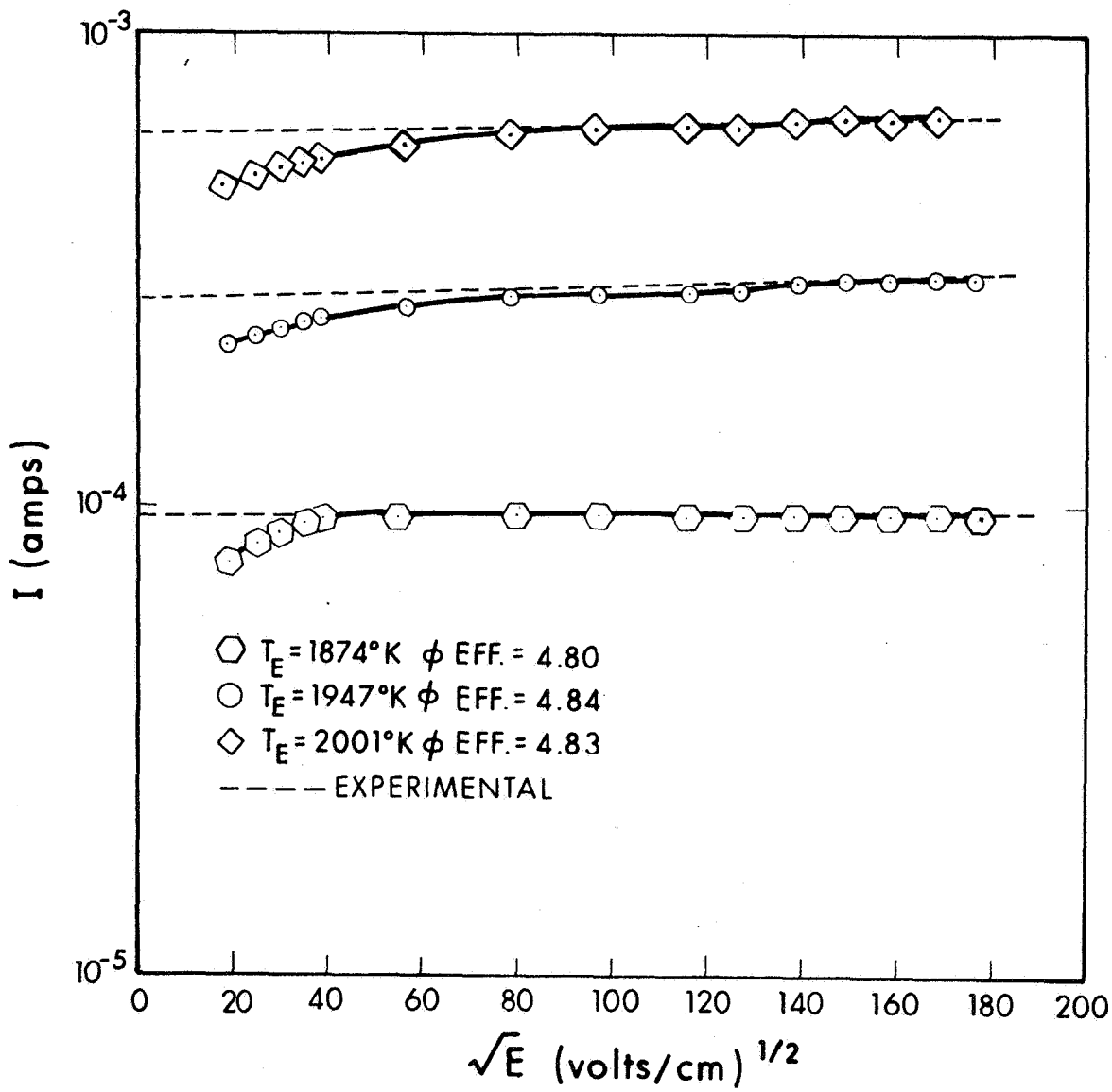

Figure 2-8. Schottky Plots of Molybdenum (110) Single Crystal; Scribe Lines on Surface as per Emission Microscope Experiments

temperatures, thereby providing values from which to calculate the electric field. On each of the curves an experimental Schottky slope was first drawn as accurately as possible through the "linear" portion of the curve. The effective work function was then computed. Figure 2-8 shows Schottky plots taken of the (110) molybdenum with the scribe lines exactly as the sample was when removed from the emission microscope. Figure 2-9 shows three Schottky plots taken of the same sample after taking a surface cut to remove the scribe lines, with subsequent fine polishing with Linde alumina A, B, and C, and a moderate electroetch in a 5 percent sulphochromic acid to remove any work-hardened material from the surface. The sample was then returned to the vacuum emission vehicle and vacuum outgassed at 2250°K for 1 hour prior to the Schottky determinations. In Fig. 2-9 experimental Schottky slopes were drawn and the work function was calculated. To determine the accuracy of the slopes experimentally extrapolated to zero field, theoretically determined slopes were superimposed upon the three curves of Fig. 2-9. The agreement is seen to be excellent. The theoretical slopes were calculated from the well-known Schottky equation:

$$\log J_{RS} = \log J_R + (1.912/T)\sqrt{E}$$

where J_R is the zero field Richardson current, and J_{RS} is the Schottky current.

Table III gives comparisons among work functions obtained from the vacuum emission vehicle, the averaged electron emission microscope measurements from Table I for the left side of the low angle grain boundary, and some recent literature values determined by Richardson plots converted to effective work functions.

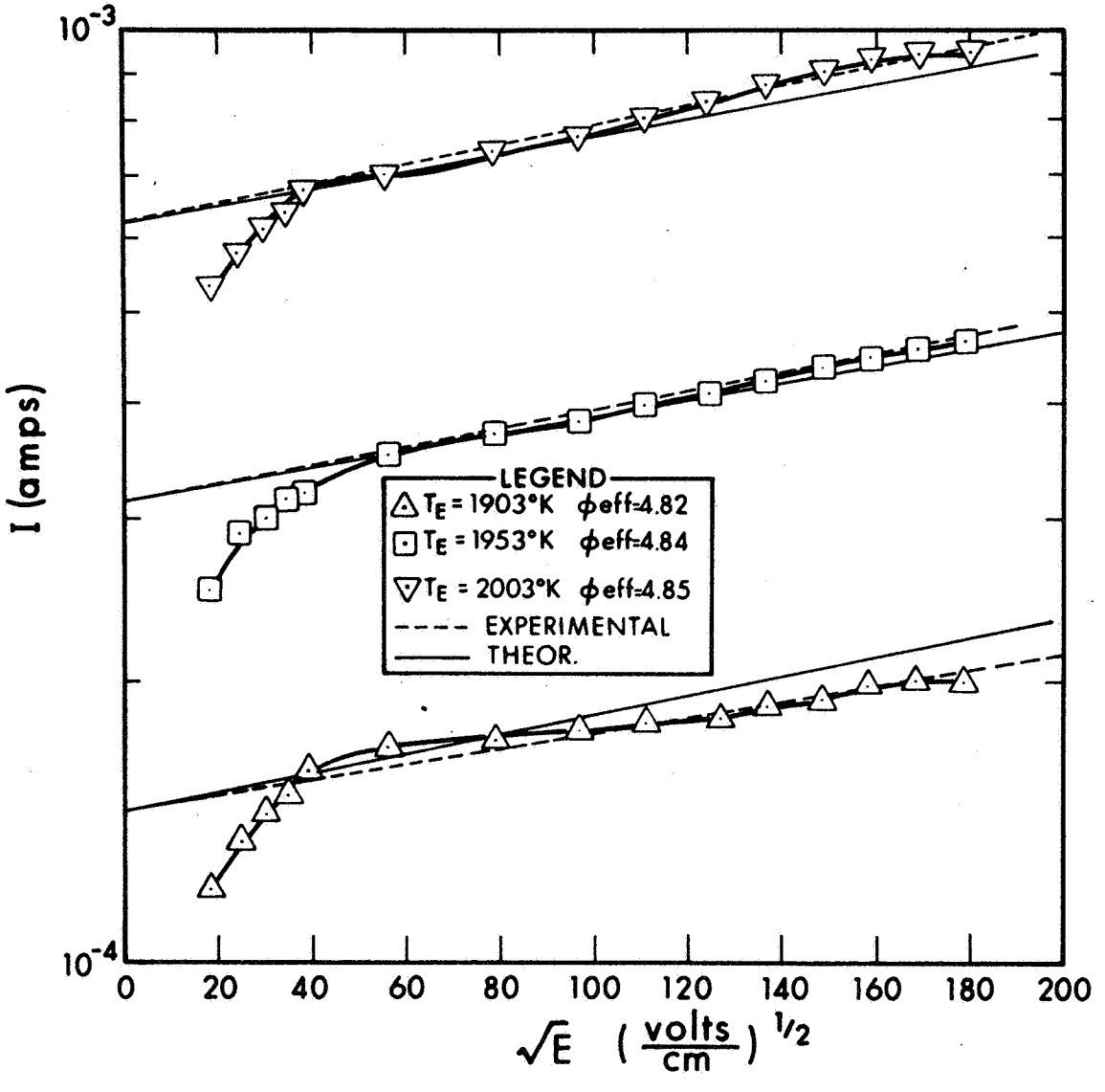

Figure 2-9. Schottky Plots of Molybdenum (110) Single Crystal, Electropolished and Vacuum Outgassed

TABLE III

COMPARISON OF EFFECTIVE WORK FUNCTION OF (110) SINGLE CRYSTAL MOLYBDENUM BY EOS VACUUM EMISSION VEHICLE, EOS ELECTRON EMISSION MICROSCOPE, AND LITERATURE VALUES

Method	T_e	ϕ_{eff} (eV)
EOS Vacuum Emission (Scribed)	2001°K	4.83 ±0.04
EOS Vacuum Emission (Scribed)	1947°K	4.84 ±0.04
EOS Vacuum Emission (Scribed)	1874°K	4.80 ±0.04
EOS Vacuum Emission (Polished and Etched)	2003°K	4.85 ±0.04
EOS Vacuum Emission (Scribed)	1953°K	4.84 ±0.04
EOS Vacuum Emission (Scribed)	1903°K	4.82 ±0.04
EOS Electron Emission Microscope	1990°K	4.90 ±0.04
EOS Electron Emission Microscope	1837°K	4.89 ±0.04
Richardson Plot (Ref. 1)	1700 - 2100°K	4.98 ±0.05
Richardson Plot (Ref. 2)	1700 - 2000°K	5.00 ±0.05
Richardson Plot (Ref. 3)	1600 - 1900°K	4.90 ±0.07

It can be seen in Table III that the difference in effective work function by vacuum emission measurements between the scribed and the polished and etched (110) molybdenum is within experimental error. But, over the temperature range, the work function of the scribed sample is consistently lower. This is reasonable and expected since it can be recalled from the emission microscope measurements that the scribed area exposed recrystallized grains of orientations different from the (110) matrix, thus grains of lower work function and higher emission capability. An exact "scribed area" could not be determined since many of the grains had already undergone secondary recrystallization and returned to the (110) matrix orientation by the conclusion of the emission microscope experiments.

The effective work function determined by vacuum emission measurements and by electron emission microscope Faraday cage measurements are seen to be within experimental error in every case. The effective work functions listed from electron emission microscope measurements are averaged over five individual Faraday cage values from different areas of the (110) single crystal matrix for each temperature indicated. The effective work functions determined in this work are within experimental error of the literature values in nearly every case. The apparently consistently lower values of the EOS emission vehicle work can be easily reconciled when it is recalled that the (110) single crystal has a low-angle grain boundary dividing the sample almost equally into two halves. The high work function side of the low-angle grain boundary yielded, by electron emission microscope measurements (from Table I), average effective work functions of 4.90 eV at 1990°K and 4.89 eV at 1837°K, well within experimental error of the listed literature values.

2.2 RHENIUM SINGLE CRYSTALS

2.2.1 X-RAY AND METALLOGRAPHIC ANALYSIS

An attempt was made by the Linde Crystal Products Division of Union Carbide to grow a boule of single crystal rhenium with the (0001) plane oriented parallel to the end face of the boule. The boule produced was unique in that the diameter was large enough so that discs could be cut off for testing and subsequent incorporation into thermionic devices of meaningful emission area. Linde Crystal Products furnished EOS with a schematic approximately reproduced at 4:1 in Fig. 2-10, showing that the boule was comprised of seven grains. Laue back reflection X-ray patterns were then produced by Linde to determine the orientation of each of the seven grains, with the results tabulated in Table IV. The relationship of the crystal plane normal of each grain with respect to the boule face normal is given by a tilt angle in the x and y directions.

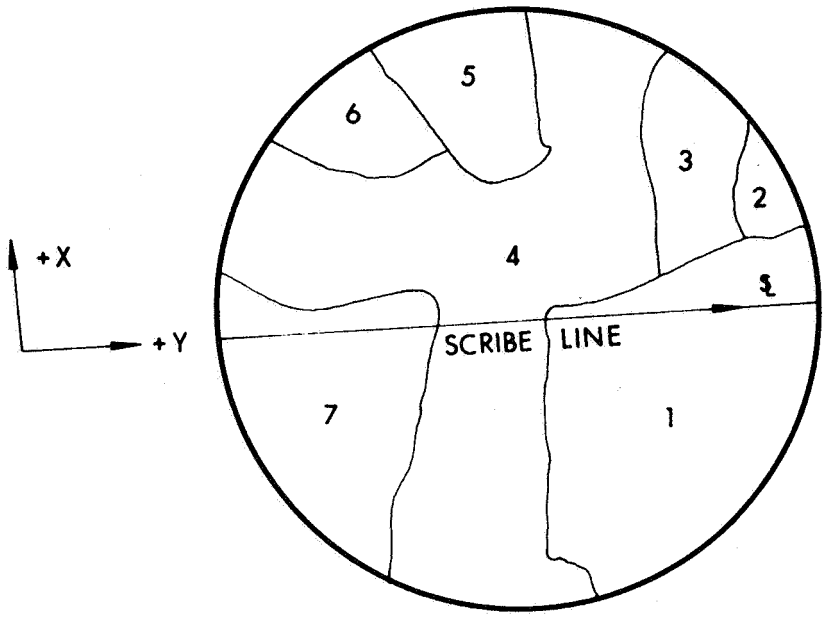

Figure 2-10. Rhenium Boule Face Sketch (4:1) Showing Seven Grains of Various Orientation

TABLE IV

RESULTS OF LAUE BACK REFLECTION DETERMINATIONS OF THE ORIENTATION OF CRYSTAL PLANE NORMALS WITH RESPECT TO THE BOULE FACE NORMAL AND SCRIBE LINE

Area	Plane Normal	Degree Tile (y)	Degree Tilt (x)	Direction of a Second Plane Normal	
1	(0001)	+6°	-4°	119° 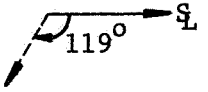	$(10\bar{1}1)$
2	$(10\bar{1}1)$	+11-1/2°	+8-1/2°	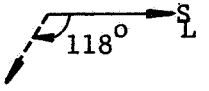	(0001)
3	(0001)	-1°	+3°	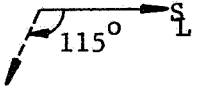	$(10\bar{1}1)$
4	(0001)	+2°	+19-1/2°	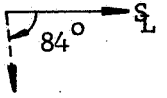	
5	(0001)	-6-1/2	+12°	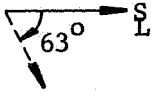	$(10\bar{1}1)$
6	(0001)	-17°	+11°	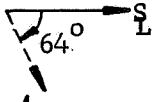	$(10\bar{1}1)$
7	$(10\bar{1}1)$	+12°	+29°	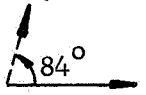	(0001)

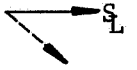

The direction in which a second plane normal lies with respect to the boule face is given by 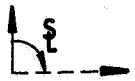

After the X-ray analysis was completed (results indicated in Table IV) it was evident that there was considerable departure of some of the grains from a (0001) boule face orientation. The boule was then mounted in a goniometer and tilted so that area #1 of Fig. 2-10 had its (0001) plane parallel to the plane of the slice and therefore parallel to the disc face. Area #1 was thus chosen to display exactly a (0001) crystal orientation. Subsequent mechanical and electropolishing exposed the grains shown in Fig. 2-11 indicating that there were a considerably larger number than originally identified. Thus, except for the larger grains such as areas #1, #4, #5, and #7, it is probable that the orientation over various regions is different from that listed in Table IV.

Figure 2-12 is a photomicrograph of rhenium sample No. 1 which had been fine polished with Linde alumina A, B, and C, and vacuum-fixed at 2150°C for two hours. After annealing, it was observed that portions of the mirror finish had apparently evaporated or diffused leaving behind a substrate exhibiting the circular machine marks assumed removed by the mechanical polishing procedures. In Fig. 2-12, the machine marks are visible and small areas that look like scales on the surface are actually areas of high polish.

As a further investigation, sample II, which was also given a fine mechanical polish, was electro-etched in a 75 percent sulfuric acid solution long enough to remove the polished layer. Figure 2-13 shows clearly that the machine marks are present in the substrate.

The conclusion drawn is that fine polishing of rhenium which has a prior work hardened surface by grinding only smears material, filling the surface irregularities, but does not remove the surface irregularities

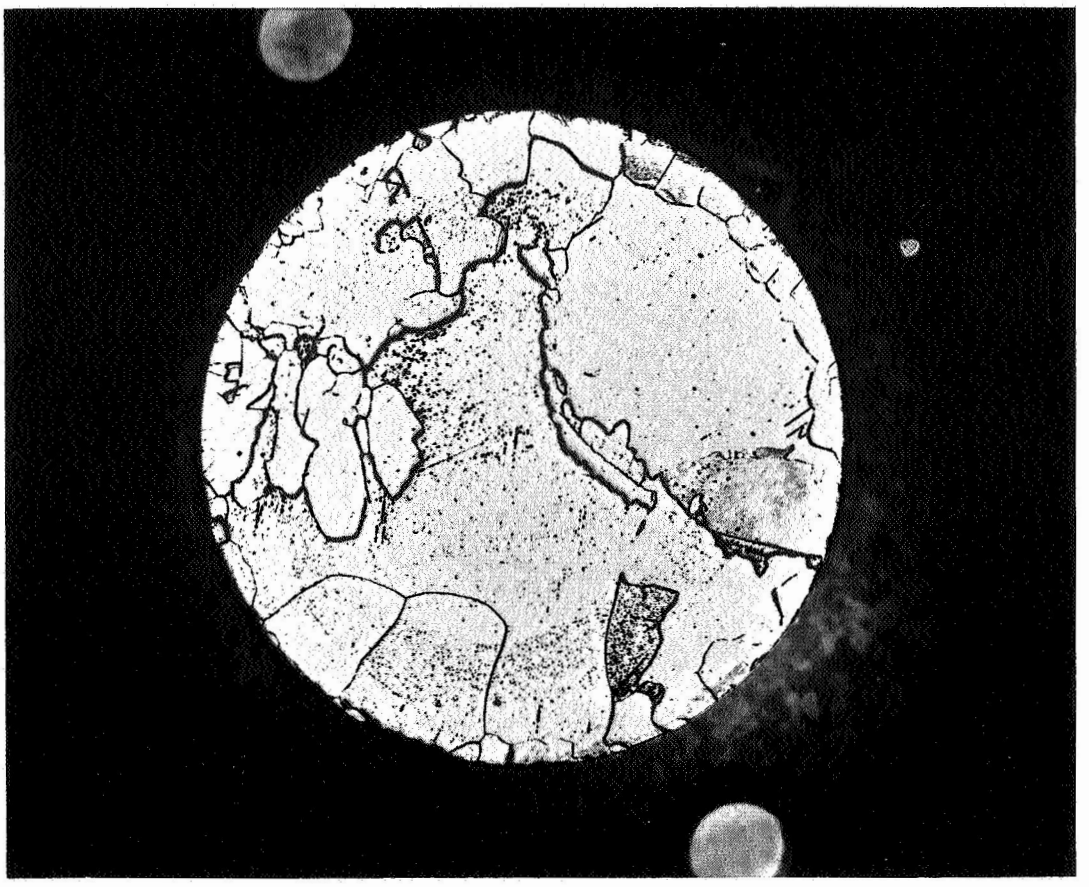

OT-668149

Figure 2-11. Rhenium Single Crystal Sample II High-Polished with Linde Alumina A, B, and C, Vacuum-Annealed at 2150°C for Two Hours, and Electropolished in a 75 Percent Sulphuric Acid Solution. Magnification 4X

005249

Figure 2-12. Rhenium Single Crystal Sample I High-Polished with Linde Alumina A, B, and C, and Vacuum-Annealed at 2150°K for 2 Hours. Magnification 10X

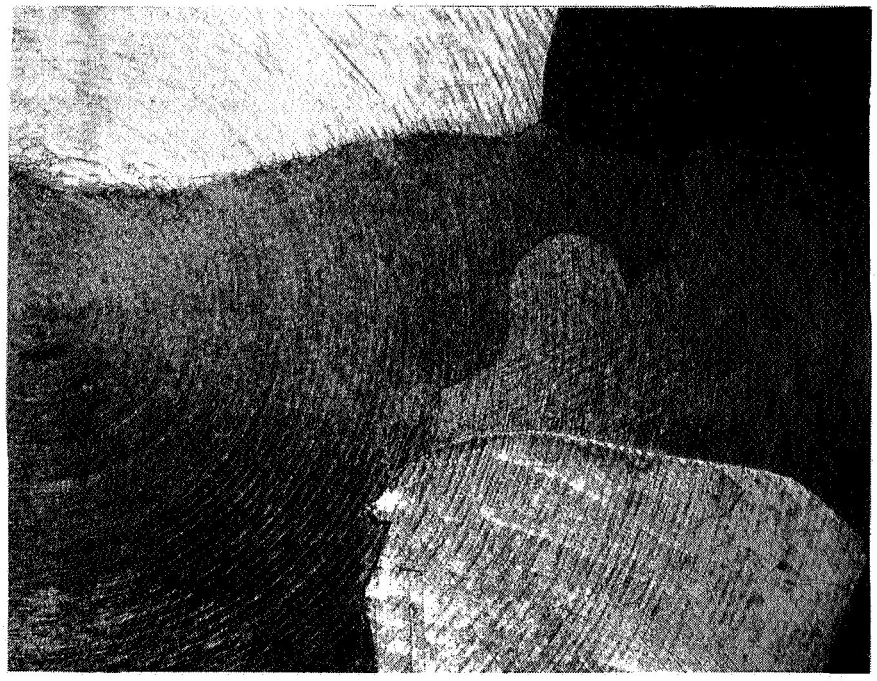

005250

Figure 2-13. Rhenium Single Crystal Sample II High-Polished with Linde Alumina A, B, and C, Electro-Etched in 75 Percent Sulphuric Acid Solution. Magnification 10X

of the work hardened layer. This is the reason that subsequent vacuum annealing gave rise to a sufficient evaporation or diffusion of the polished surface layer to expose the now fully annealed grinding ridges. Thus, to insure that a smooth surface remains after vacuum annealing, a series of coarse to fine polishing papers should be used to remove the grinding ridges before fine polishing. Electropolishing before fine polishing may also achieve the same results. In Fig. 2-11 the grinding ridges were removed by electropolishing. The sample was already fully annealed at 2150°C for 2 hours.

2.2.2 ELECTRON EMISSION MICROSCOPE INVESTIGATION OF SINGLE CRYSTAL RHENIUM

Rhenium sample II was electropolished and mounted in the electron emission microscope. The area identified in photomicrograph Fig. 2-14 corresponds to the electron emission micrograph composite of Fig. 2-15. The numbered grains on Fig. 2-14 correspond to the numbered grains on the sketch of Fig. 2-10. Each emission micrograph of the composite of Fig. 2-15 was accompanied by a Faraday cage current measurement from which the work function was calculated. In Table V, those measurements taken within grains No. 1 and 4 corresponding to the composite area are listed. The averaged effective work function for grain No. 1 (which is supposed to be exactly a (0001) crystal orientation) is 5.26 eV. The averaged effective work function of grain No. 4 is 4.92 eV. It is of interest to note that Wichner and Pigford[4] have reported an effective work function for (0001) rhenium of 5.56 eV from experiment. It, therefore, appears that grain No. 1 reportedly cut to exhibit the (0001) crystallographic plane is, in actuality, off axis.

Accompanying the composite of Fig. 2-15 are three electron emission current profiles, their locations shown by the lines drawn through the composite. Approximate average effective work function values are indicated by various sections of the profiles. High plateaus on the

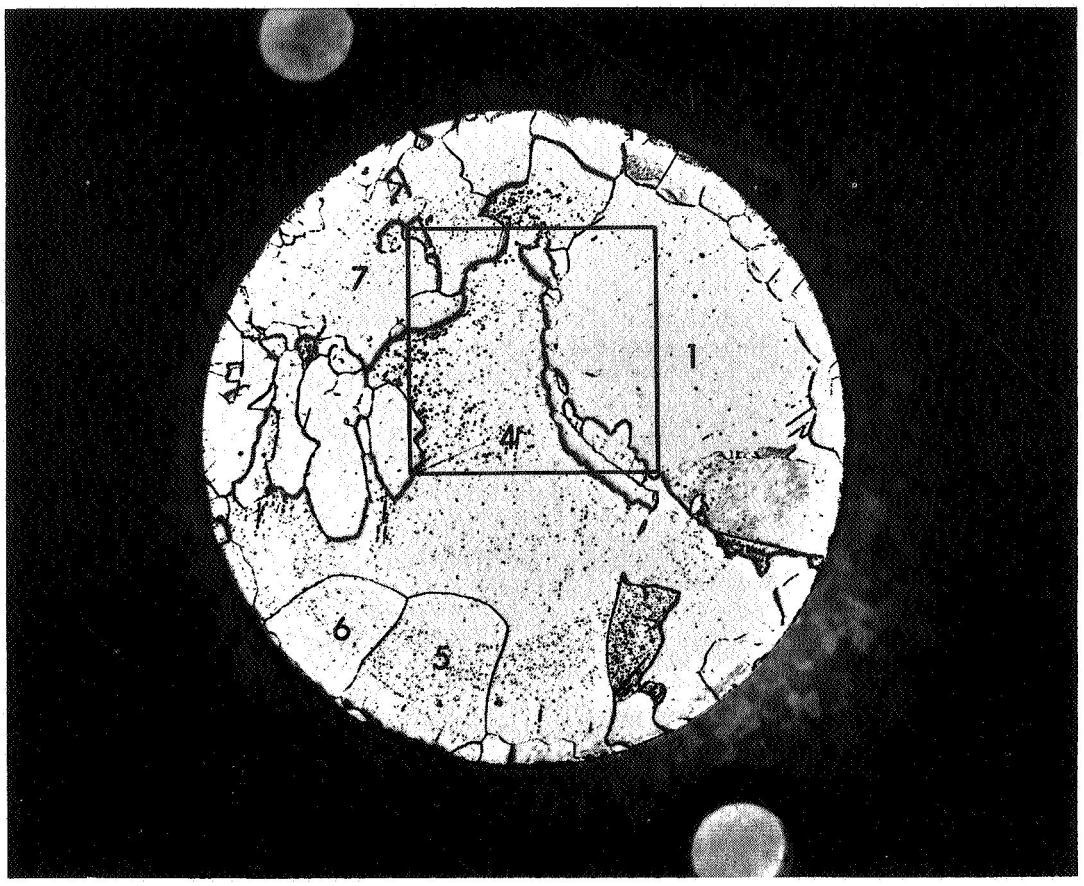

OT-668149

Figure 2-14. Photomicrograph of Rhenium Sample II High-Polished with Alumina A, B, and C, Vacuum-Annealed at 2150°C for Two Hours, and Electropolished in a 75 Percent Sulphuric Acid Solution. Magnification 4X

TABLE V

EFFECTIVE WORK FUNCTION OF GRAINS NO. 1 AND 4 (SAMPLE II) CORRESPONDING TO EMISSION MICROGRAPHS OF THOSE AREAS SHOWN IN FIG. 2-15 COMPOSITE. MAGNIFICATION 86X. TEMPERATURE 2053°K.

Grain No. 1		Grain No. 4	
J_o amps/m^2	ϕeV	J_o amps/m^2	ϕeV
0.729	5.23	4.28	4.92
0.774	5.22	4.19	4.92
0.61	5.27	4.92	4.89
0.674	5.25	4.37	4.91
0.647	5.27	3.92	4.94
0.565	5.28	3.10	4.97
0.483	5.31	4.28	4.92
0.638	5.25	2.87	4.99
0.574	5.27	3.73	4.96
0.524	5.28	5.28	4.88
0.506	5.30	4.83	4.89
0.583	5.27	4.128	4.92
0.574	5.27	4.64	4.91
0.528	5.29	4.01	4.93
0.473	5.31	3.82	4.94
		3.64	4.95
0.492	5.30	4.28	4.92
0.465	5.31	3.73	4.94
0.520	5.29	4.19	4.92
0.546	5.28	3.84	4.94
0.546	5.28	3.66	4.94
0.510	5.29	4.84	4.94
0.555	5.28	3.82	4.94
0.611	5.26	2.91	4.99
0.665	5.25	3.20	4.96
0.601	5.27	3.64	4.95
0.701	5.24	3.64	4.95
0.783	5.22	4.01	4.93
0.783	5.22	4.01	4.93
0.692	5.24	3.96	4.93
0.729	5.23	3.46	4.95
0.747	5.23	3.46	4.94
0.856	5.20	3.10	4.98
		3.11	4.97
		3.0	4.98
		3.05	4.98
		2.73	5.00

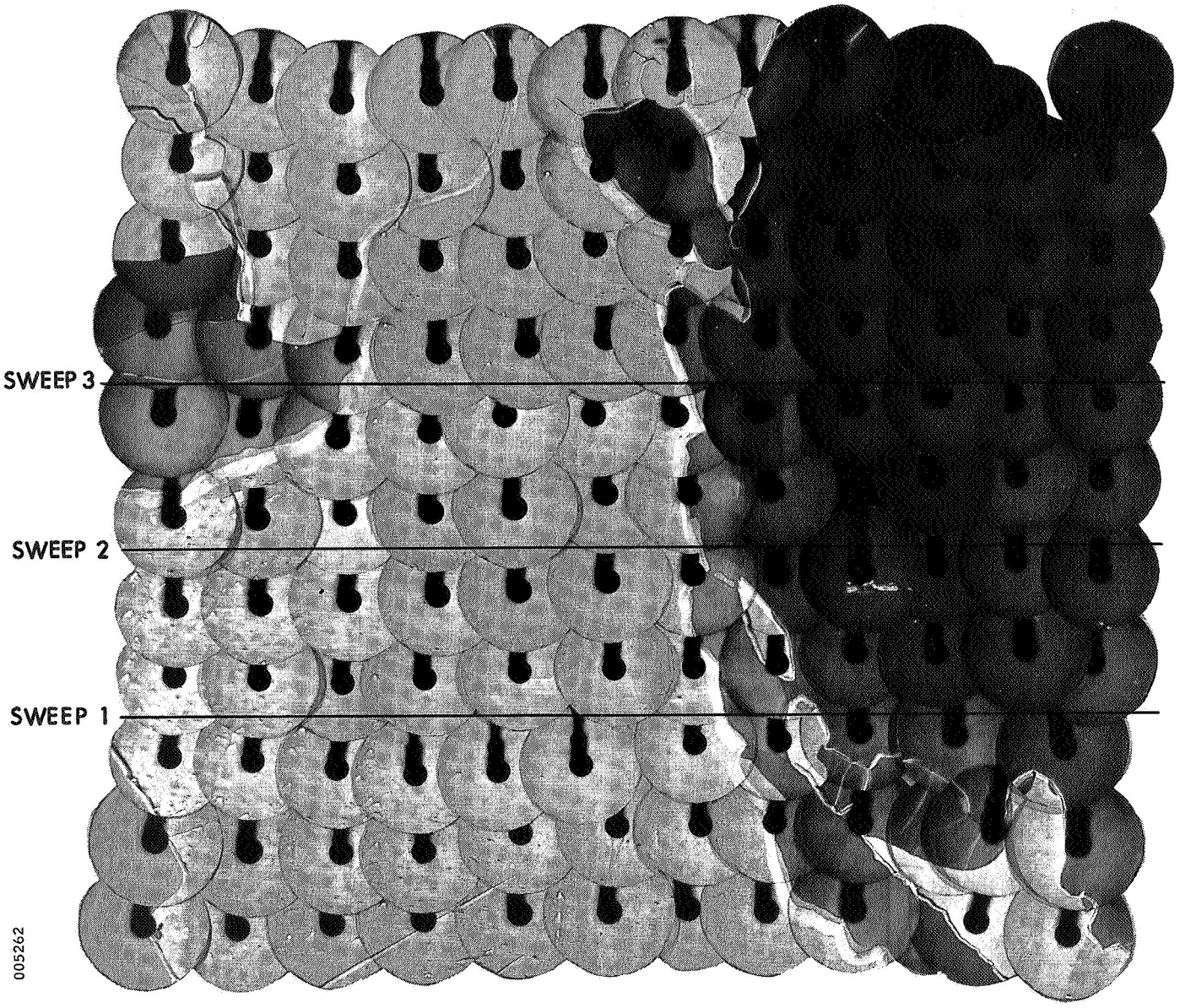

Figure 2-15. Mapped Composite of Rhenium Single Crystal Sample II Area with Current Profiles. Magnification 86X

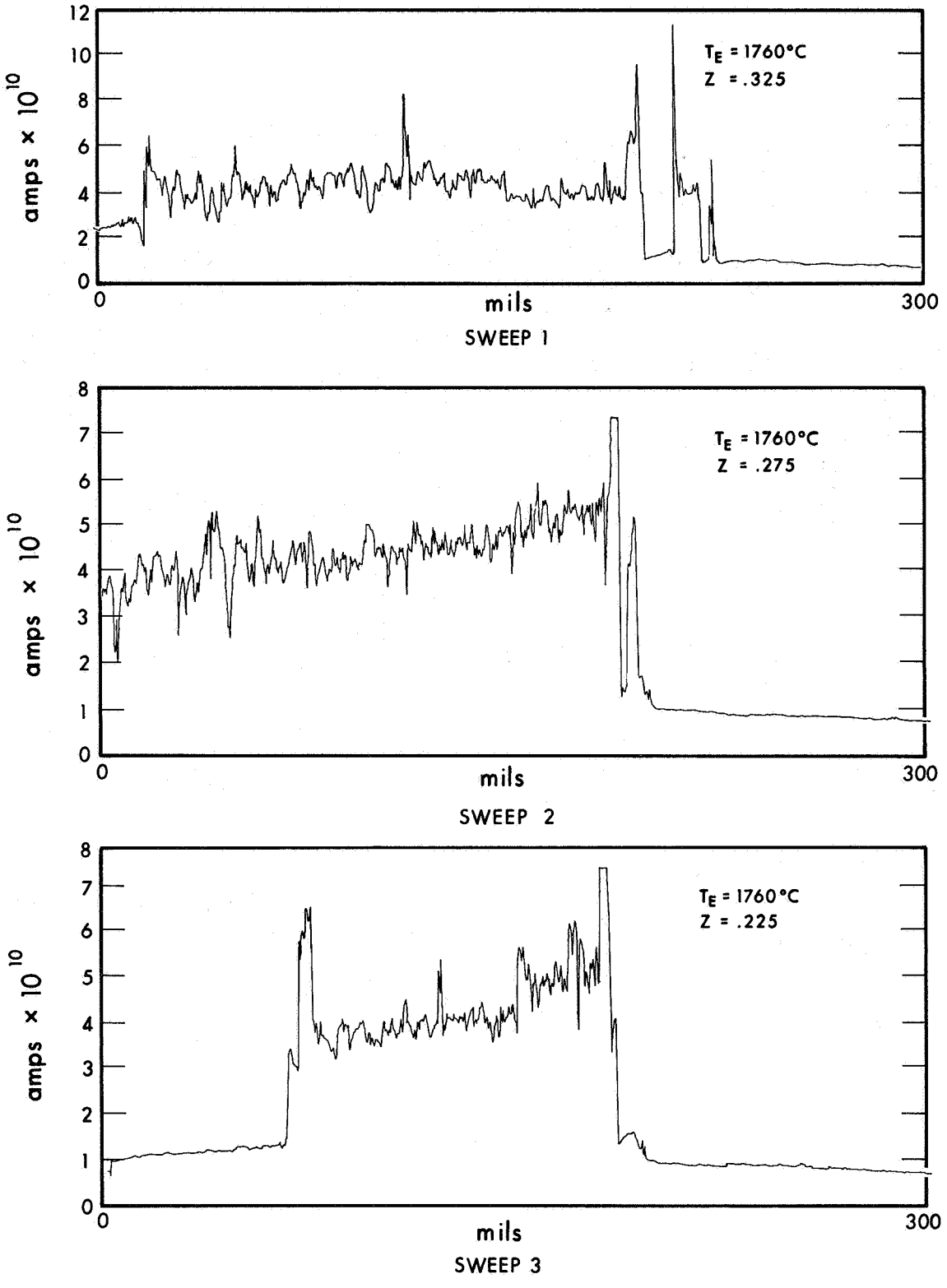

005268

Figure 2-15. Mapped Composite of Rhenium Single Crystal Sample II Area with Current Profiles. Magnification 86X (contd)

profiles denoted grain boundary exhibited values of current greater than that shown on the diagram due to limitations of the current scale.

The dark areas of the composite can be seen to correspond to low current emission and therefore high work function, while the light areas exhibit high emission and low work functions. The transition region from a low emission area to a high emission area (or vice versa) does not appear extremely sharp, the reason being that wide grain boundary regions have been created by electropolishing. This effect can be observed on the scans and compared with the same region of the composite.

In general, the work functions indicated in Table V are the same as those on the current profiles for the particular grains examined (i.e., No. 1 and 4.).

2.2.3 VACUUM EMISSION MEASUREMENTS OF SINGLE CRYSTAL RHENIUM

The effective work function of the rhenium was determined experimentally by vacuum emission vehicle measurements after the various surface preparations mentioned in Subsection 2.2.1: (1) polished with Linde A, B, and C alumina powders to a mirror finish, (2) polished as in (1) and electroetched, (3) polished as in (1) and electropolished. After all surface preparations, the samples were chemically cleaned in hydrochloric acid and triple-boiled in distilled water. Each sample was then vacuum-annealed at 2150^{o}C for 2 hours before vacuum emission tests were begun.

Figures 2-16, 2-17, and 2-18 are Schottky plots corresponding to the three preparations mentioned. The effective work functions are within experimental error (±0.04 eV) in every case for a given temperature, indicating that the surface preparations do not have any significant effect upon the experimental results. Table VI is a resume of the data of Figs. 2-16, 2-17, and 2-18.

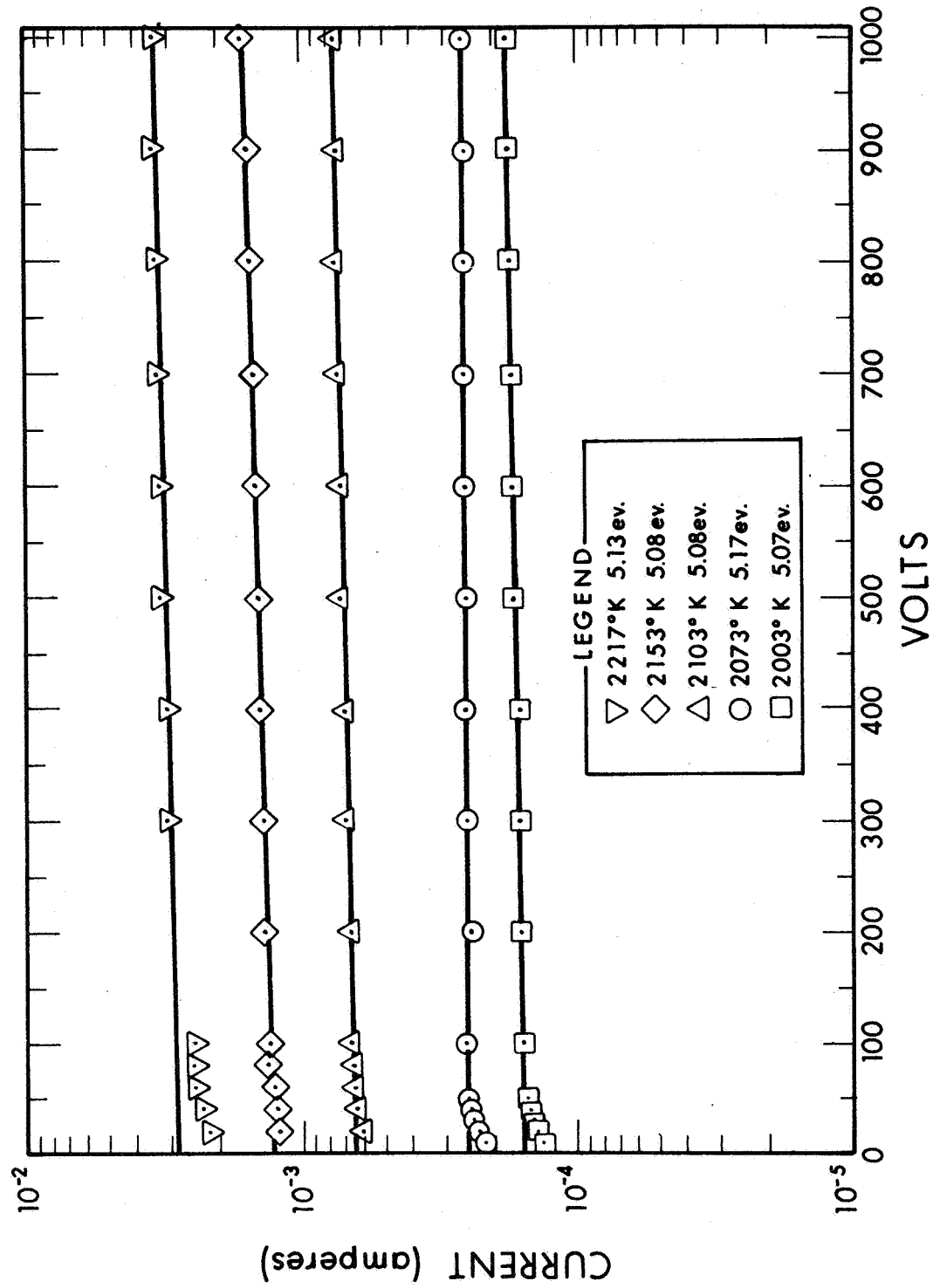

Figure 2-16. Effective Work Function Determinations of Single Crystal Rhenium I by Vacuum Emission Vehicle Measurements (polished and high-fired for 2 hours at 2150°K)

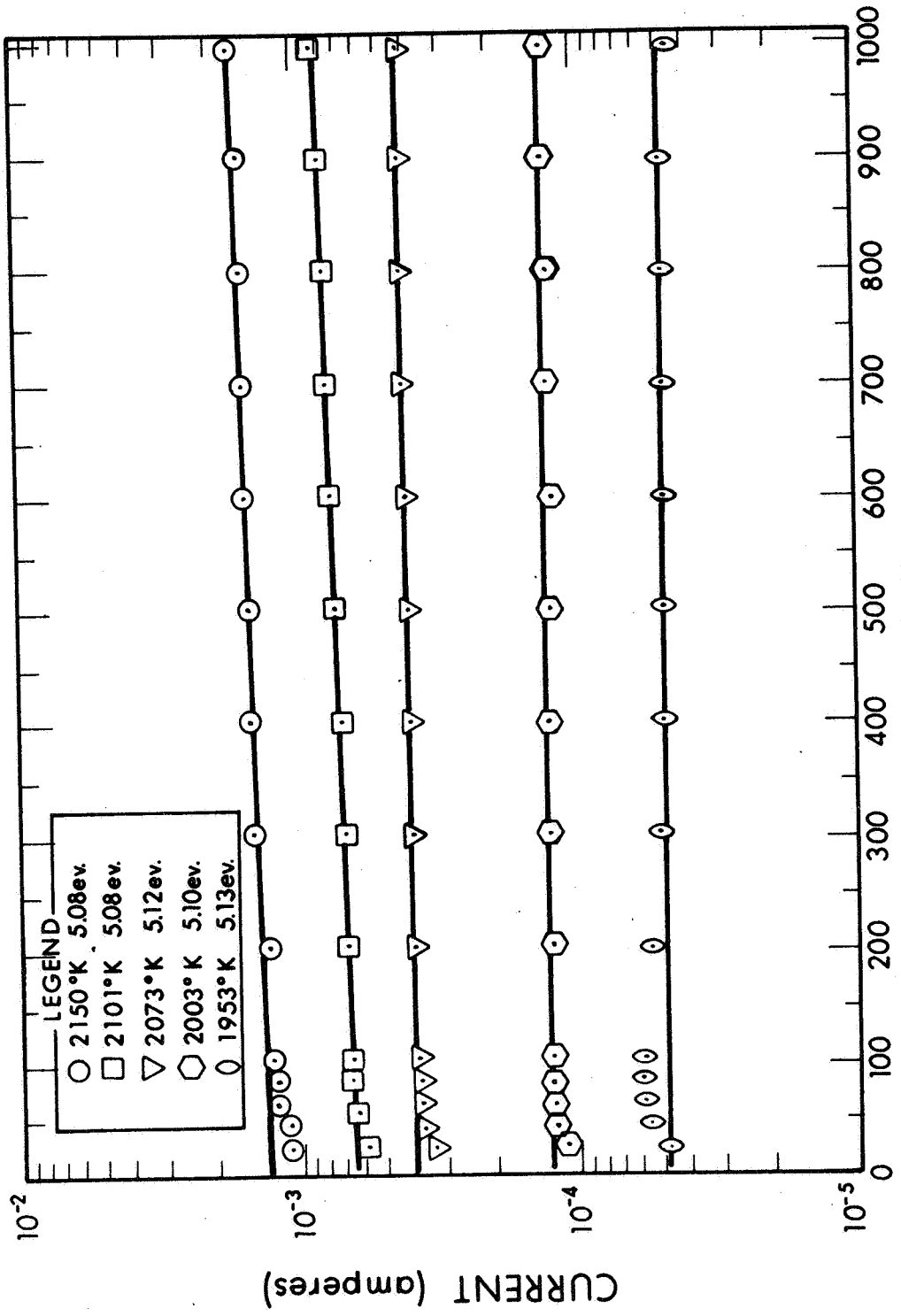

Figure 2-17. Effective Work Function Determinations of Single Crystal Rhenium Sample II by Vacuum Emission Vehicle Measurements (polished, electro-etched, and high-fired for 2 hours at 2150°K)

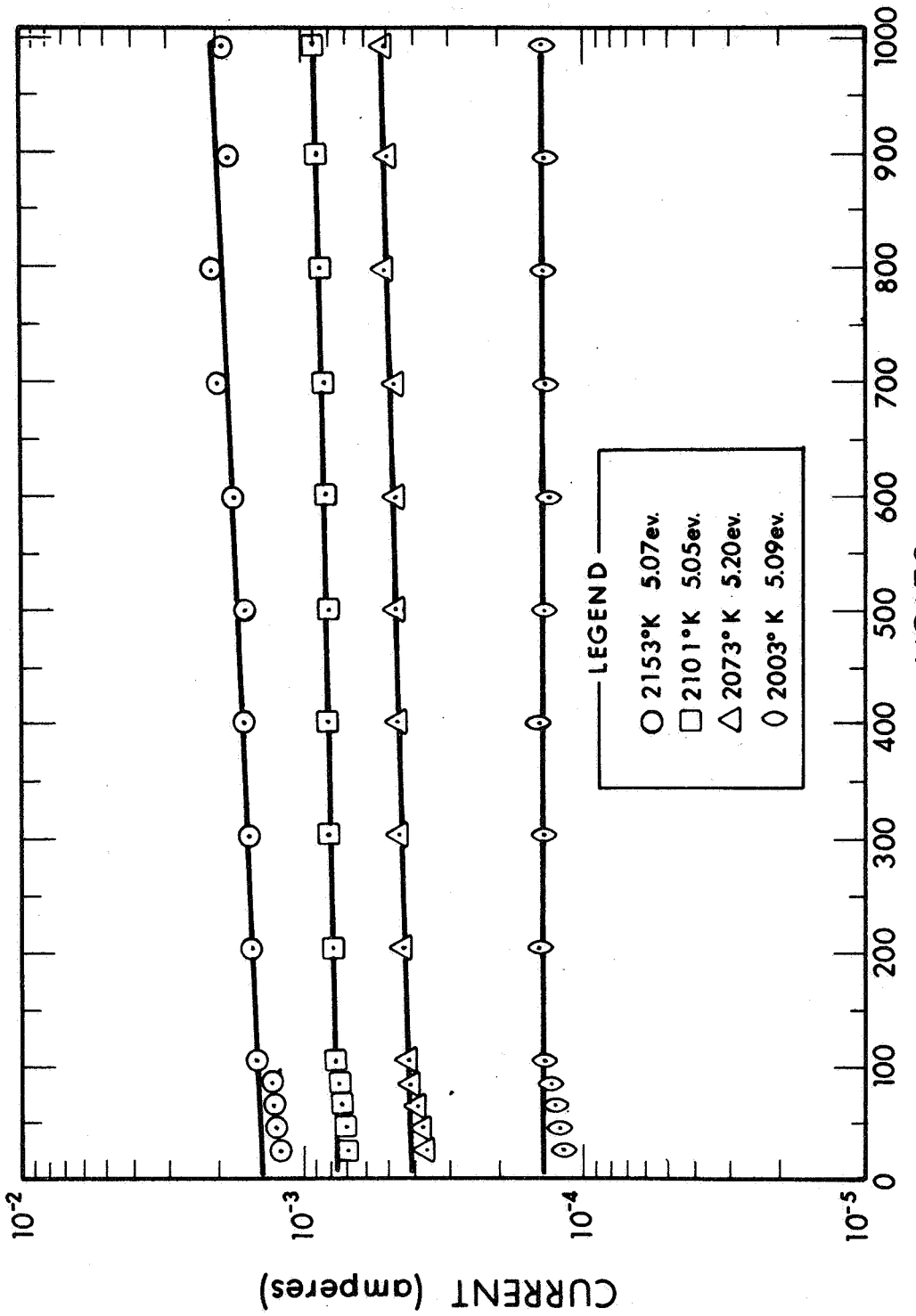

Figure 2-18. Effective Work Function Determinations of Single Crystal Rhenium Sample I by Vacuum Emission Vehicle Measurements (electropolished and high-fired for 1 hour at 1900°C)

TABLE VI

EFFECTIVE WORK FUNCTION ϕ_{eff}* FOR RHENIUM SINGLE CRYSTALS SAMPLE NO. I AND II FROM VACUUM EMISSION VEHICLE MEASUREMENTS

$T^{o}K$	Fine Polish (I)	Fine Polish Electroetch (II)	Fine Polish Electropolish (I)
1953		5.13	
2003	5.09	5.10	5.09
2073	5.20	5.12	5.20
2101	5.05	5.08	5.05
2153	5.07		5.07
2.50		5.08	

*Estimated ϕ_{eff} ±0.04 eV.

Since grains No. 1 and 4 in sample II together constitute well over 50 percent of the surface examined, it is probably valid to attempt some comparisons between the electron emission microscope results and the vacuum emission vehicle test results. In Subsection 2.2.2, the averaged effective work function from electron emission microscope measurements for grain No. 1 was found to be 5.26 eV, and for grain No. 4, 4.92 eV. The average of these two numbers is 5.09 eV, which compares very favorably with the vacuum emission results reported in Table VI. Because of the large number of grains, a more precise comparison between the two methods of investigation was found to be impractical.

The results of these measurements show that the rhenium samples investigated here exhibit an effective work function which is no higher, and in most cases lower, than those reported in earlier work[5] on vapor deposited rhenium.

2.3 VAPOR-DEPOSITED RHENIUM VARIABLE PARAMETER TEST VEHICLE

A variable parameter test vehicle with vapor-deposited rhenium electrodes was fabricated and performance tested. Vapor-deposited sample II was the emitter and vapor-deposited sample IV, the collector.

The interelectrode spacing and parallelism in the variable parameter vehicle are established by independently applying a force to three spring-loaded rods of a differential thread drive mechanism. Contact between the emitter and collector is indicated by a drop in the output voltage of the device. When momentary or slight contact is made, the emitter temperature decreases and the collector temperature increases.

The first task consisted of optimizing the dc current output of the vehicle as a function of spacing, cesium reservoir temperature, and collector temperature. The optimizations of current were performed at two different output output voltages and emitter temperatures which were selected for comparison to previously tested thermionic converters. Figure 2-19 shows the results of the current optimization for an emitter temperature of 1800^{o}K and a constant voltage output of 0.4 volt. Figure 2-20 shows the current optimization for an emitter temperature of 1700^{o}K and a voltage output of 0.3 volt.

The complete optimization at a fixed output voltage and constant emitter temperature consisted of three parts. First, the collector temperature was held constant, the spacing was fixed, and the cesium reservoir temperature was varied to achieve maximum output current. Second, the spacing was fixed again, but at a different value, while the collector temperature was held constant as before. The cesium reservoir temperature was again varied to obtain maximum current output. The second step was repeated for three or four interelectrode spacings while the cesium reservoir temperature achieved optimized current output. Third, the collector temperature was varied, performing steps one and two for each temperature. Thus, for a given emitter temperature and constant

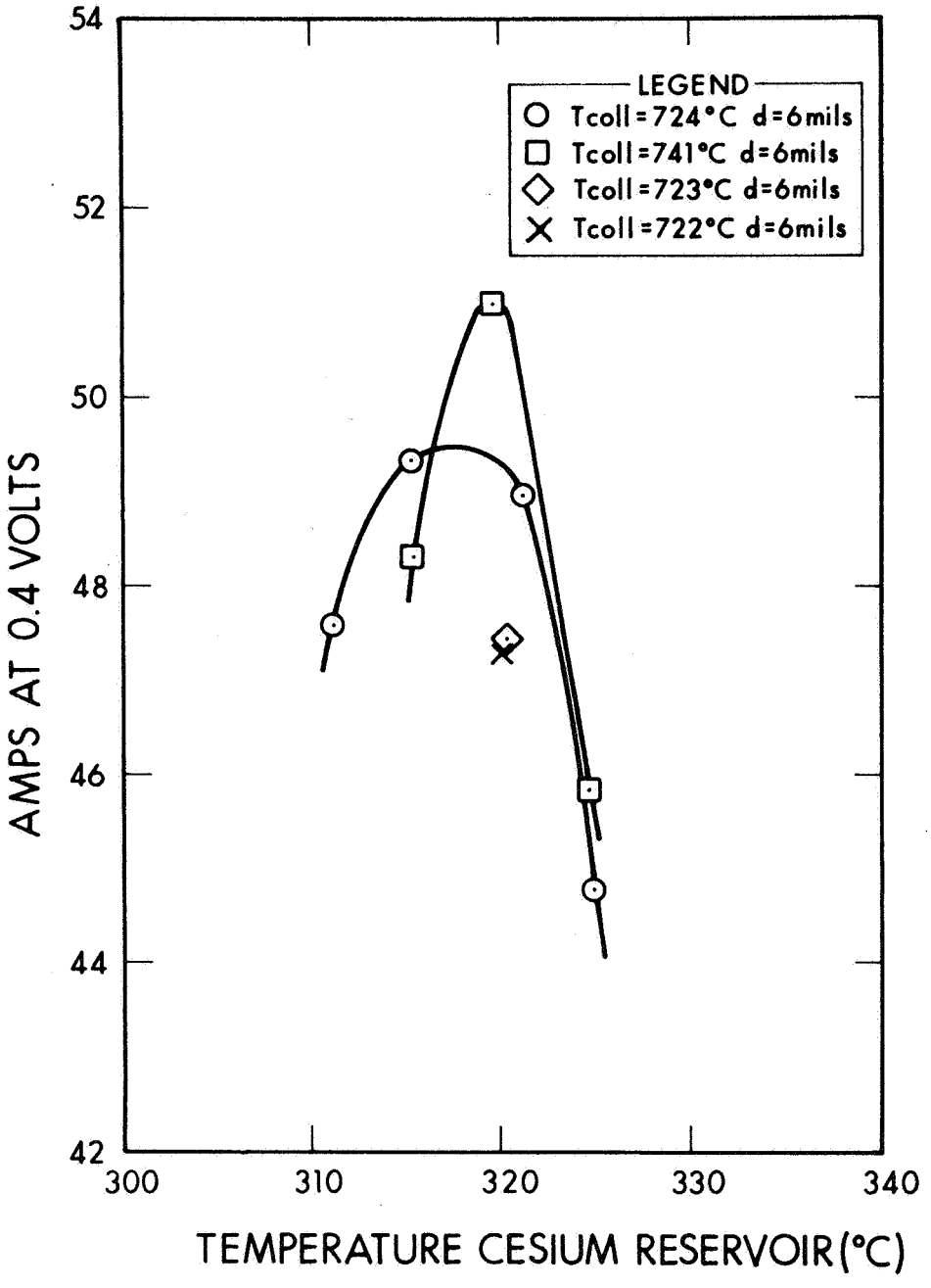

Figure 2-19. Vapor-Deposited Rhenium Variable Parameter Test Vehicle Optimized for Converter S/N 109 Type Performance, for an Emitter Temperature of 1798°K and a Voltage Output of 0.4 Volt

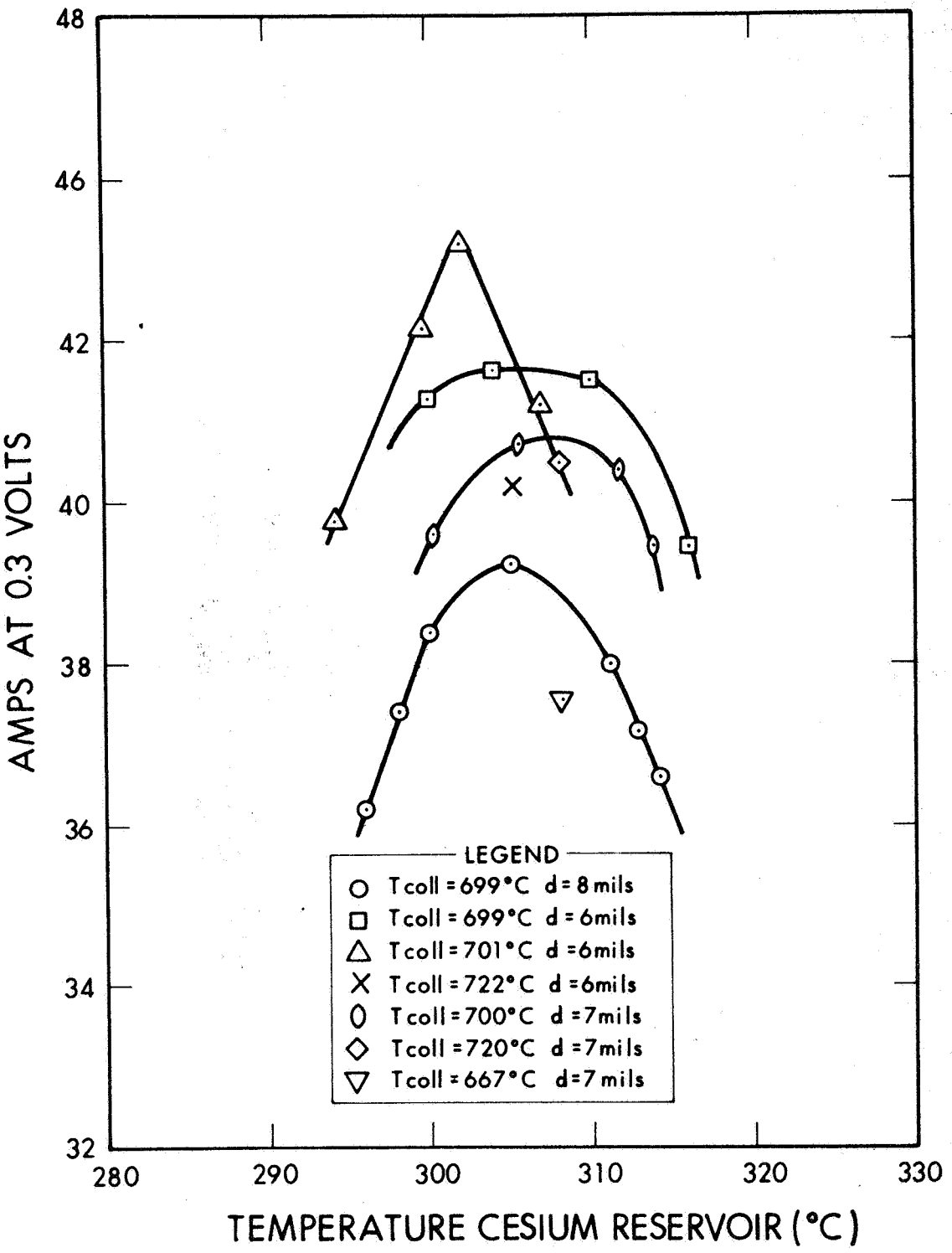

Figure 2-20. Vapor-Deposited Rhenium Variable Parameter Test Vehicle Optimization for Converter S/N 110 Type Performance, for an Emitter Temperature of 1700°K and a Voltage Output of 0.3 Volt

output voltage, the above procedure produced a complete set of optimization data from which the maximum output current could be obtained as a function of the variables: spacing, collector temperature, and cesium reservoir temperature.

The second task consisted of obtaining output voltage (V) versus interelectrode spacing (d) curves for comparison with the polycrystalline rhenium emitter, polycrystalline rhenium collector system, and the polycrystalline rhenium emitter-molybdenum collector system curves as shown in Fig. 2-19. The collector temperature ($\approx$ 720 $\pm$10^{o}C), emitter temperature (1735 $\pm$5^{o}C), cesium reservoir temperature (330 $\pm$1^{o}C), and current (38A) were the same for all three curves. A comparison of the vapor-deposited rhenium electrode system with the polycrystalline rhenium electrode system shows that the performance is very nearly the same. However, from the beginning of operation, it was very difficult to determine exactly where the emitter-collector short would occur with 0.3-0.5 mil. Consequently, the region of the curve of increasing voltage at spacings less than approximately 0.5 mils is almost nonexistent on the vapor-deposited rhenium curve. Moreover, electrode parallelism was difficult to establish with 0.3-0.5 mil, and electrodes not in parallel also exhibit curves lacking an "upturn" in the electron space charge region.

From the beginning of operation, it was very difficult to determine exactly when the emitter-collector short would occur as the voltage would drop slowly rather than abruptly to zero as electrode contact was made. Spacing was therefore extremely difficult to set as was the parallelism of the electrodes. Approximately 300 hours of testing were accomplished before it was concluded that the problem was internal to the vehicle.

Before the flanges were cut to open the system, the cesium was frozen out in the reservoir by keeping the reservoir in liquid nitrogen while

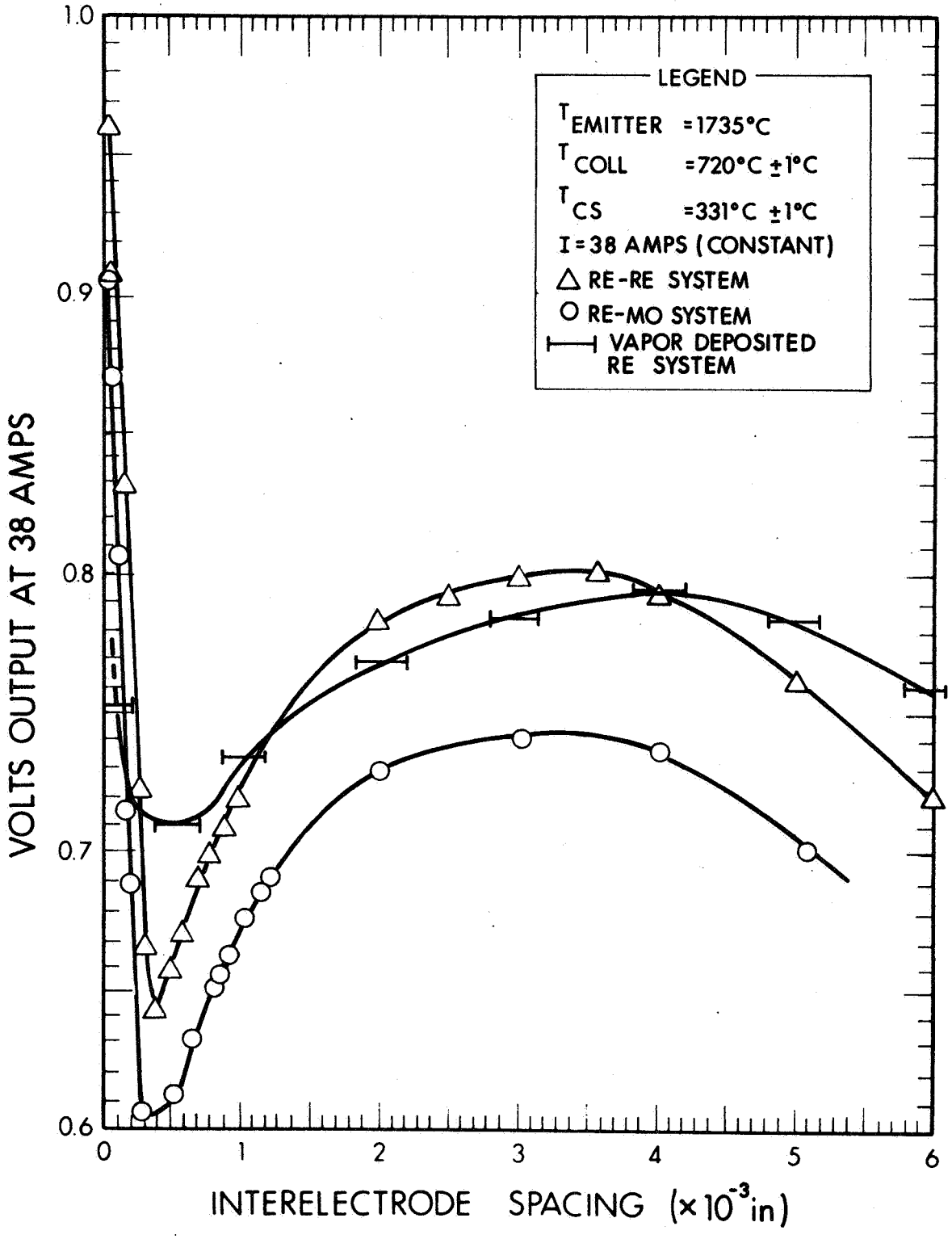

Figure 2-21. Comparison Plot of Re-Re, Re-Mo, and Vapor-Deposited Re-Vapor-Deposited Re Systems Showing Voltage Output Difference of 0.060 to 0.080 Volt Over Entire Spacing Range

heating the body of the test vehicle with a hot air gun. The cesium tubulation was then cut open, accompanied by a fire flash as the cesium oxidized. The device was then leak checked and found to be leak-tight.

Upon opening the test vehicle, it was found that the emitter, collector, and guard ring surface had been partially joined together during final assembly. During operation and thermal cycling the electrodes subsequently parted, but the electrode surfaces were disrupted in such a way that small projections of metal would make contact and short the electrodes before the plane of the surfaces actually touched. A microscopic examination revealed that the surface projections were almost a mil above the electrode surface. This is consistent with operational difficulties in the 0.5 mil to 0.8 mil spacing range.

SECTION 3

LOW TEMPERATURE (1700°K-1800°K) CYLINDRICAL CONVERTER (TASK III)

Four cylindrical converters consisting of vapor-deposited rhenium electrodes are being designed and fabricated to provide performance comparison to planar converters of the same electrode material developed under NASA Contract NAS7-514. An identical emitter area of 2.0 cm^2 and collector area of 1.88 cm^2 will provide an exact comparison between the two geometries.

The cylindrical converters (S/N 109CA, 109CB, 110CA, and 110CB) were designed for maximum performance at the emitter temperatures and interelectrode spacings specified below:

		Design Criteria	
Converter Designation	Emitter Temperature	Interelectrode Spacing	Power Output
SN109CA, 109CB	1800°K	6 ±0.6 mils	10.5 W/cm^2
SN110CA, 110CB	1700°K	10 ±1 mils	4.5 W/cm^2

The EOS concept of cylindrical converters is readily adaptable to radioisotopic and out-of-pile thermionic systems. Basically, this concept allows the individual converters to be externally connected for series-parallel choice hookup. Moreover, each converter contains a separate reservoir which allows for individual converter testing and optimization.

As a conceptual application of the cylindrical converter, Fig. 3-1 depicts a five-converter heat pipe array with an estimated electrical output of 100 watts at 2.0 volts. Ten such arrays emanating from a

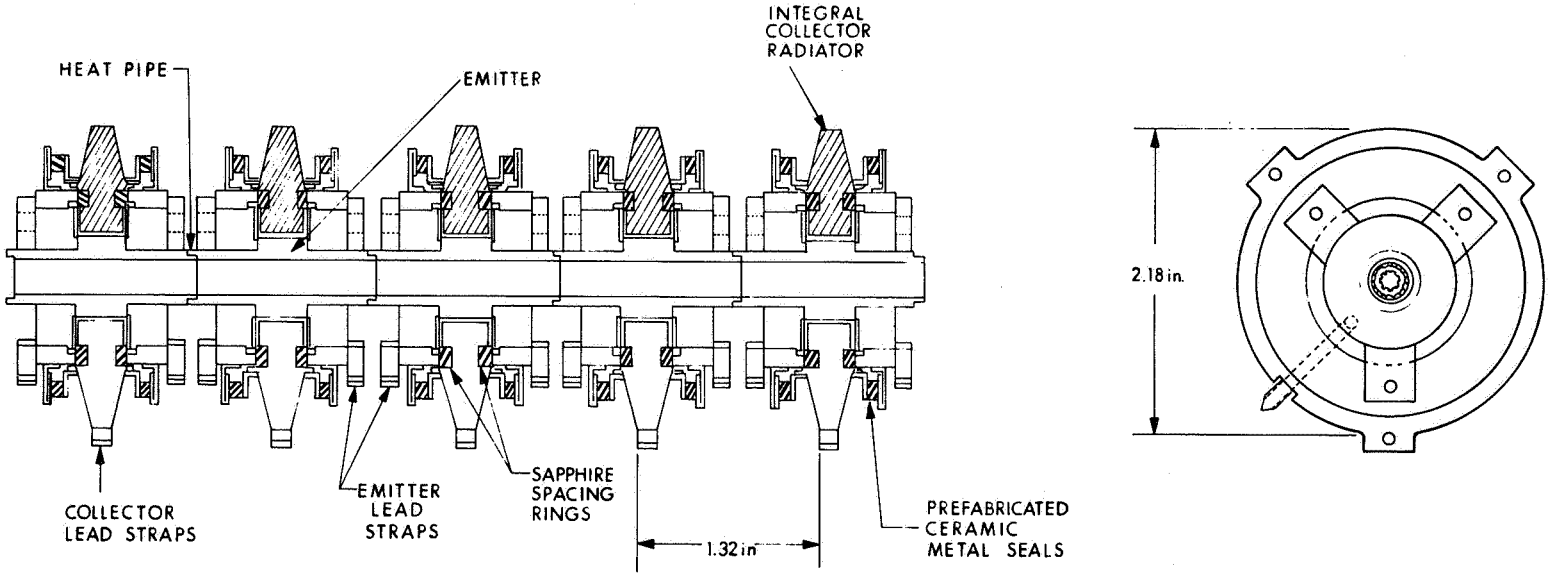

Figure 3-1. Potential Application of EOS Cylindrical Converter (Multiconverter Array)

common heat source could provide an unconditioned power of 1 kW (e). The key features of the five-converter array are: a segmented heat pipe joined by electron beam welding prealigned cylindrical converters, cast sapphire trilayer insulation, and a completely pretested component system in the same manner as the SET generator.

3.1 CONVERTER DESIGN

The design of the cylindrical converter has been completed. Figure 3-2 shows the converter design. There are four major subassemblies: (1) the emitter, (2) the emitter support structure, (3) the collector-radiator, and (4) prefabricated ceramic-to-metal seals. All major subassemblies are electron beam welded together to form the final converter configuration.

3.1.1 EMITTER SUBASSEMBLY

The emitter subassembly of the converter is formed by the vapor deposition of rhenium on a molybdenum mandrel. After the deposition process, the mandrel is removed by chemical etching. The final dimensions of the cylindrical emitter are obtained by precision grinding. Figure 3-3a shows the emitter of S/N 109CA.

As a design iteration, an emitter will be fabricated which forms a section of a segmented heat pipe. This will be formed by machining a fluted mandrel so that a replication of the grooves will form channels on the inside diameter of the emitter subassembly. A cross section of this emitter is shown in Fig. 3-3b. At each end of the segmented emitter, steps are made to allow joining (by electron beam welding) to next section of the segmented heat pipe (Ref. Fig. 3-1).

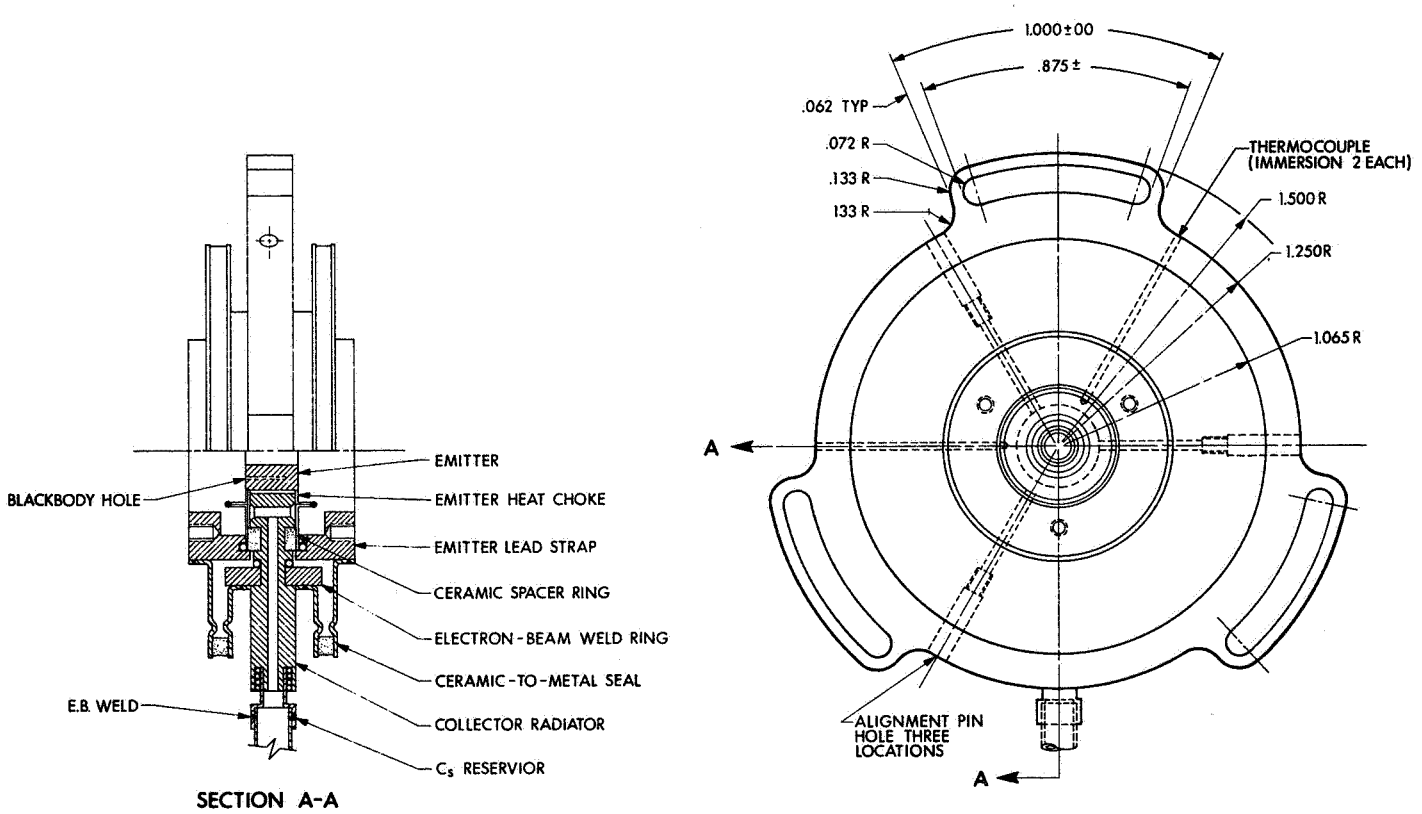

Figure 3-2. Cylindrical Converter Assembly

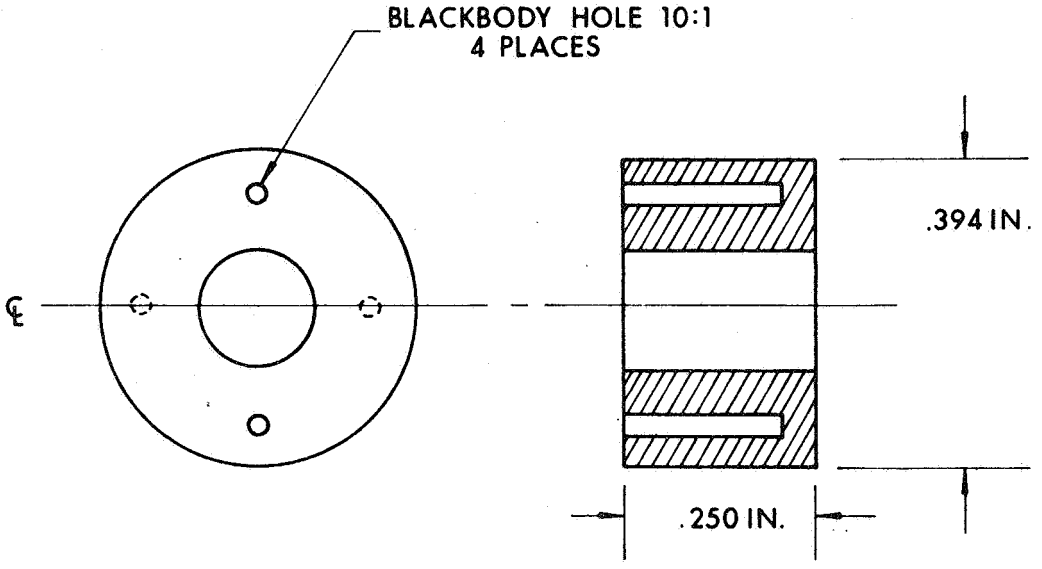

Figure 3-3a. Vapor-Deposited Rhenium Cylindrical Converter Emitter (S/N 109CA)

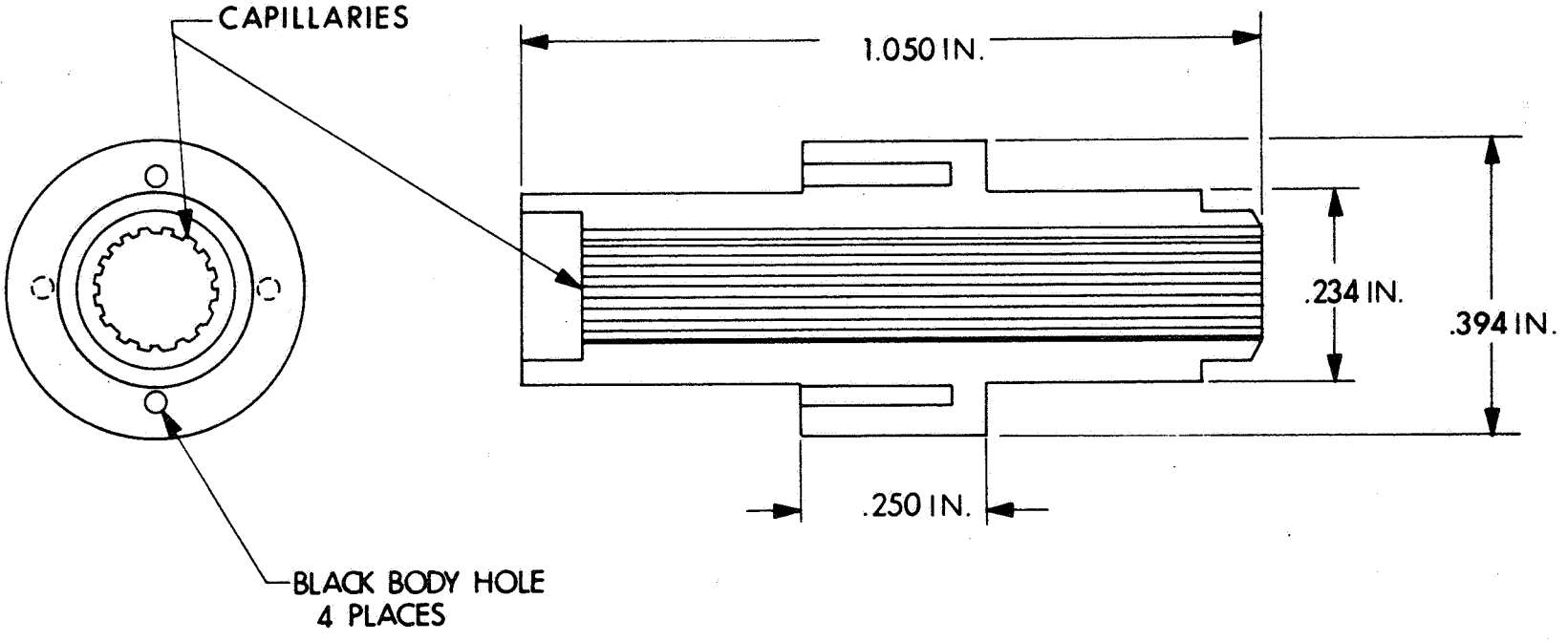

Figure 3-3b. Vapor-Deposited Rhenium Emitter - Segmented Heat Assembly

3.1.2 EMITTER SUPPORT STRUCTURE

The thermal design for the emitter support structure, which is normally referred to as an envelope, must: (1) act as an effective heat choke, thermally isolating the 1800°K emitter from the other structural members of the converter, such as the ceramic-metal seals, (2) provide the converter current path without large voltage drop over the length of the envelope; and (3) maintain mechanical integrity and leak tightness. The heat choke design requires balancing the electrical losses with the thermal losses. The ratio of electrical to thermal loss α can be written as:

$$\alpha = I^2 \frac{\rho(L/A)}{K_{\Delta T}\left(\frac{A}{L}\right) - \frac{1}{2}\rho\left(\frac{L}{A}\right)}$$

(where radiation losses have been omitted in the first order approximation).

In practice, the L/A ratio must be obtained to minimize α.

For cylindrical geometry, the above equation is:

$$\alpha = \frac{I^2 \rho \ln (r_o/r_i)}{2\pi \ell} \frac{K_{\Delta T} 2\pi\ell}{\ln (r_o/r_i)} - \frac{I^2 \rho \ln (r_o/r_i)}{4\pi \ell} \qquad (1)$$

where I is the total current passing through the envelope, ρ is the resistivity of the material, ℓ is the thickness of the material, r_i is the inside radius, r_o is the outside radius, ΔT is the temperature drop across the heat choke envelope, and K is the thermal conductivity of the material.

In addition to the thermal design, the emitter support structure must be considered from a materials selection standpoint. It has been previously demonstrated that the selection of a rhenium emitter is an

a priori selection of a rhenium support structure to insure long-life high temperature compatibility of both members.

The emitter support structure for S/N 109CA design parameters are:

ℓ = 0.0127 cm (0.005 in. thick)
I = 50 amps
ρ = 80×10^{-6} cm-ohm
K = 0.48 W/cm-^{o}K (rhenium)
$\Delta T \simeq 750^{o}$
r_i = 0.45 cm
r_o = 1.2 cm

Substituting the above values into Eq. 1, the total thermal power conducted down the envelope is 58 watts, and the total joule heating of the heat choke is 2.5 watts. Therefore, the total power lost down the heat choke by conduction is $\simeq$ 56 watts for an emitter temperature of 1800^{o}K with a current of 50 amperes flowing in the emitter.

The emitter support structure is a 0.005-in.-thick rhenium annulus which is titanium brazed to a niobium emitter lead strap on the outer diameter of the annulus and electron beam welded on the inside diameter to the emitter. Since the support structure is simply a plate with a hole in the middle operating at 1700^{o}K-1800^{o}K and constrained at a perimeter which operates at 1000-1100^{o}K, there is the probability of warpage.

Two support structure designs are being considered:

1. The first approach employs a straight annular ring without a convolute. Figure 3-4a shows this design.

   To determine whether or not thermal expansion will cause excessive warpage, a thermal mockup of this structure was fabricated and tested.

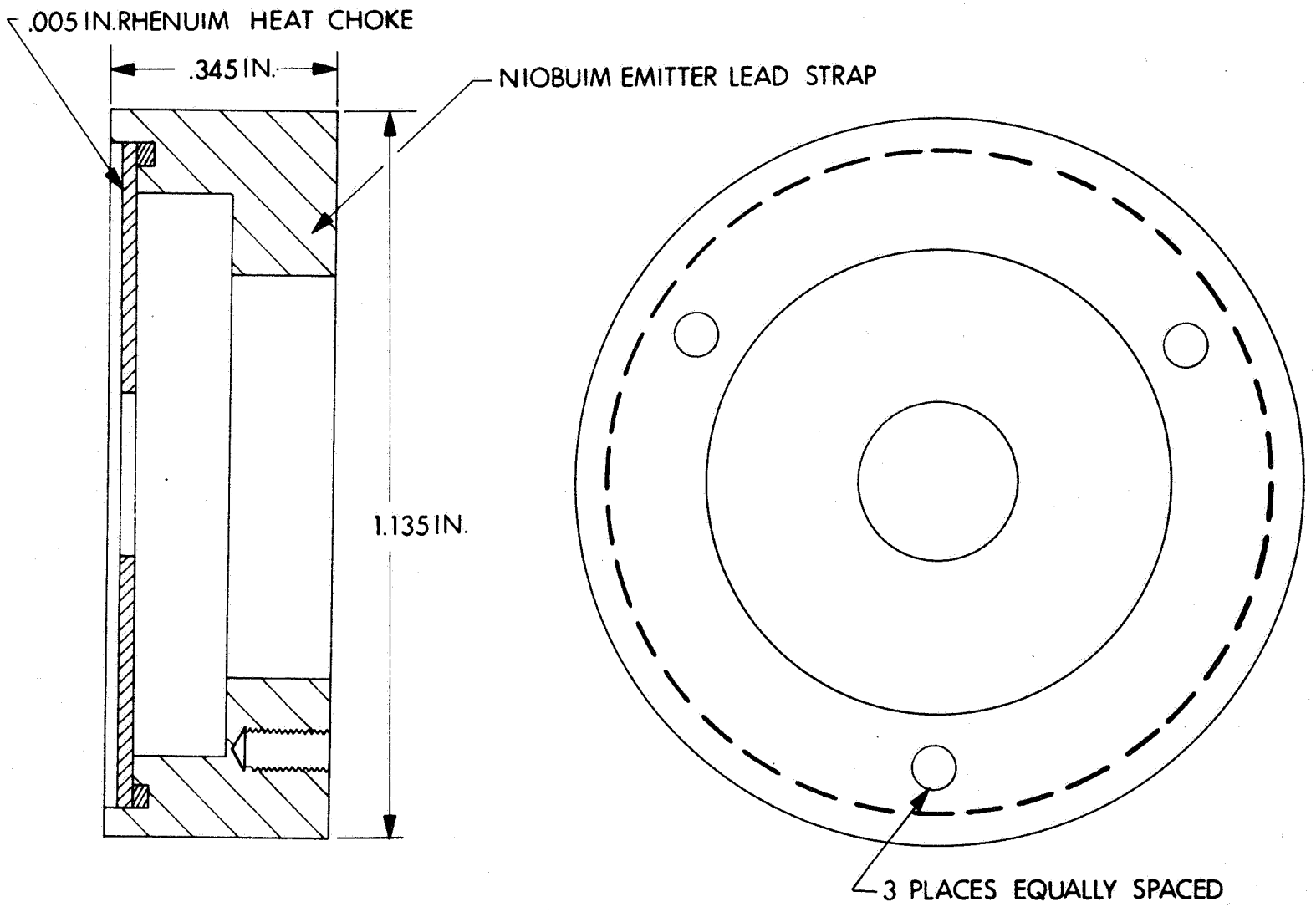

Figure 3-4a. Emitter Heat Choke Envelope (Annular Ring)

The results of this test showed that this approach is feasible with the addition of sapphire spacing rods between the envelope and the collector-radiator assembly.

The no-convolution annular ring approach has one distinct advantage; it is a simple geometry which lends itself to standard fabrication techniques.

2. The alternate design approach that EOS is considering is shown in Fig. 3-4b in which the support structure incorporates a single convolution to act as a bellows for the radial thermal expansion.

   To form a single convolution bellows structure of rhenium presents fabrication problems. Rhenium, unlike tantalum and niobium, work-hardens rapidly during cold forming operations. Therefore, more exotic fabrication techniques must be employed such as special dies, interstage annealing between each reduction, and special machining fixtures to accommodate the convolution design.

3.1.3 COLLECTOR-RADIATOR STRUCTURE

The collector-radiator is a circular molybdenum plate which forms an integral unit. Figure 3-5 is a photograph of a finish-machined collector-radiator. The radiator portion of the assembly is shown with a high emittance (0.78) coating of Rokide "C". The radiating area shown is ≈ 40 cm^2 total for two sides.

The collecting surface (inside diameter) is coated with a 0.020-in.-thick vapor deposited rhenium surface. The area of current collection is 1.88 sq cm^2 corresponding to the EOS planar converters.

One problem area peculiar to cylindrical converters is the eccentricity of electrodes. Where measurements have been reported, interelectrode spacings of 5 to 7 mils are sometimes concentric to within only 3 mils. EOS' experience in testing variable-spaced planar electrodes indicates that skew electrodes can reduce potentially available power output densities by as much as 25-30 percent (the performance comparison of planar and cylindrical geometries is valid as long as electrode dimensions are much greater than interelectrode spacing).

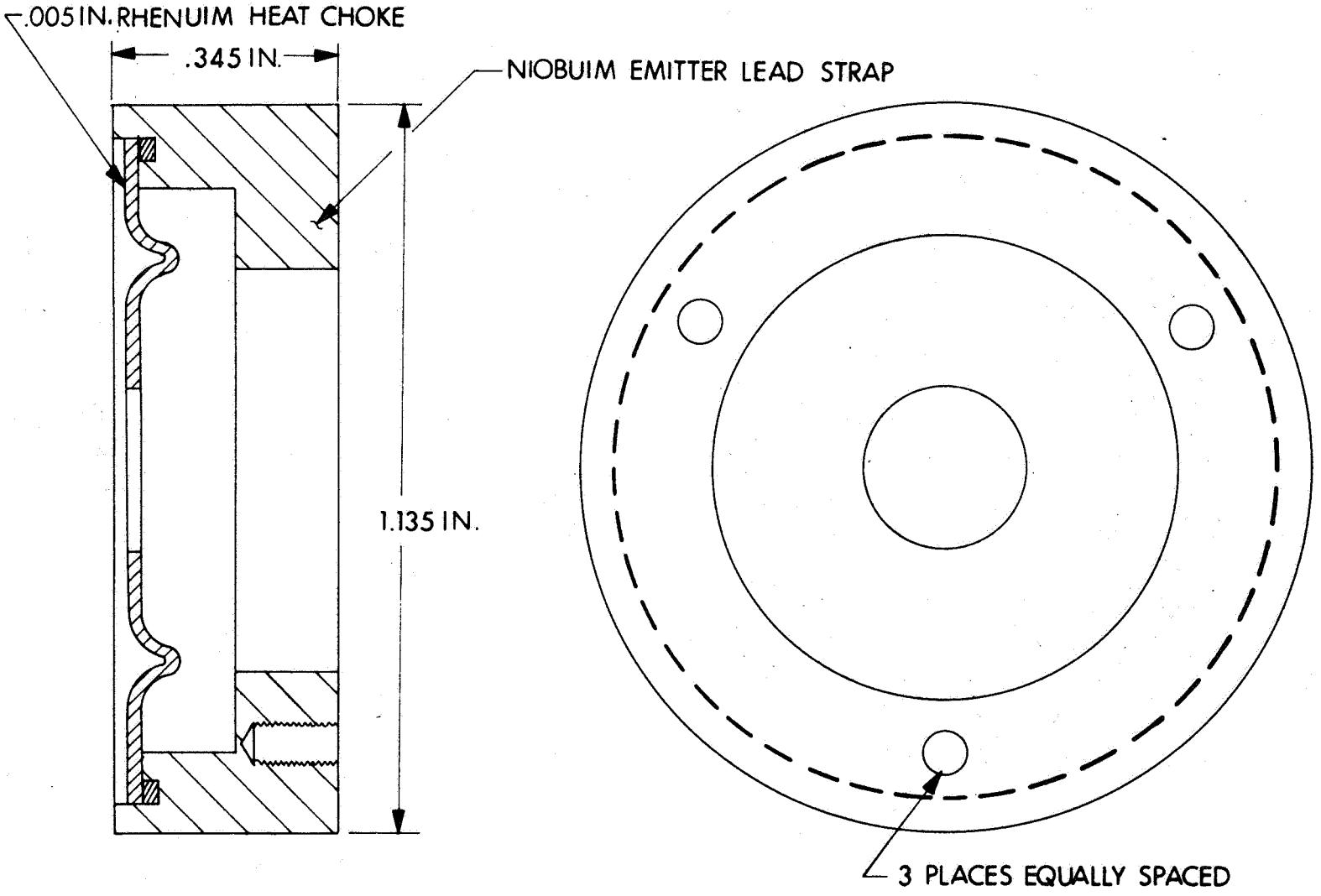

Figure 3-4b. Emitter Heat Choke Envelope With Convolution

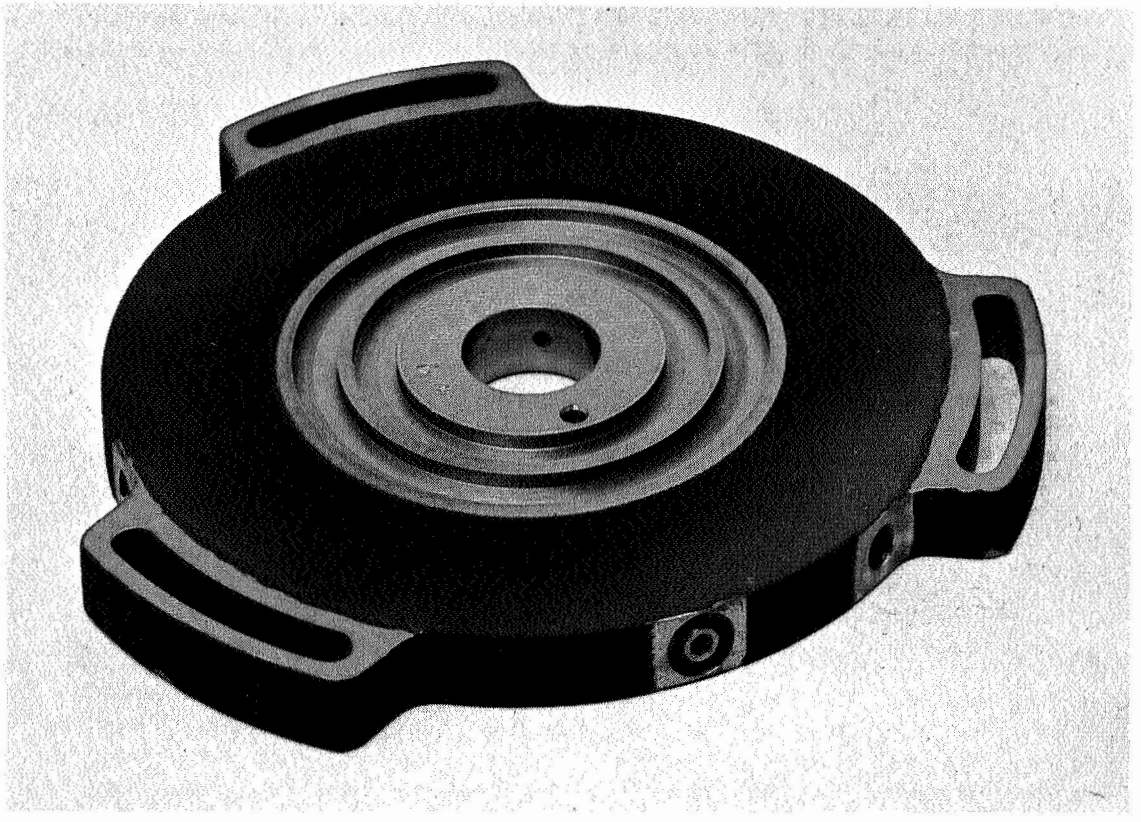

SP-66873

Figure 3-5. Cylindrical Converter Integral Molybdenum Collector-Radiator Assembly

Therefore, EOS has incorporated into the design a method to establish and retain the concentricity of electrodes during the fabrication processes. Figure 3-6 is a drawing of the collector-radiator assembly. The three holes drilled radially and placed 120^{o} apart are alignment pinholes. Pins are placed into the holes to precisely set the emitter concentric to the collector. The subassemblies of the converter are electron beam welded with the pins in place. The pins are then removed and the holes are plugged and electron beam welded shut to form a vacuum-tight diode assembly.

Three other radial holes are drilled: one is for region transfer; the other two are for temperature measurements of collector surface via immersion thermocouples. The weight of the integral collector-radiator is 176 grams.

For the collector-radiator design, it is necessary to calculate the collector heat load that the radiator must reject at the design operating point of 53 amperes (i.e., approximately 21 watts for 1.88 cm^2 at 0.40 volts).

The collector heat load, Q total, is the sum of three terms:

$$Q_{total} = Q_{el\ ht} + Q_{rad} + Q_{cs\ cond}$$

The first term, $Q_{el\ ht}$ is the heat generated by the drift electron current as it dissipates the energy acquired by falling through the potential of the collector work function plus the random potential energy in the plasma, i.e.,

$$Q_{el\ ht} = I\ (\varphi_{coll} + \epsilon\ kT_{pl}/e)$$

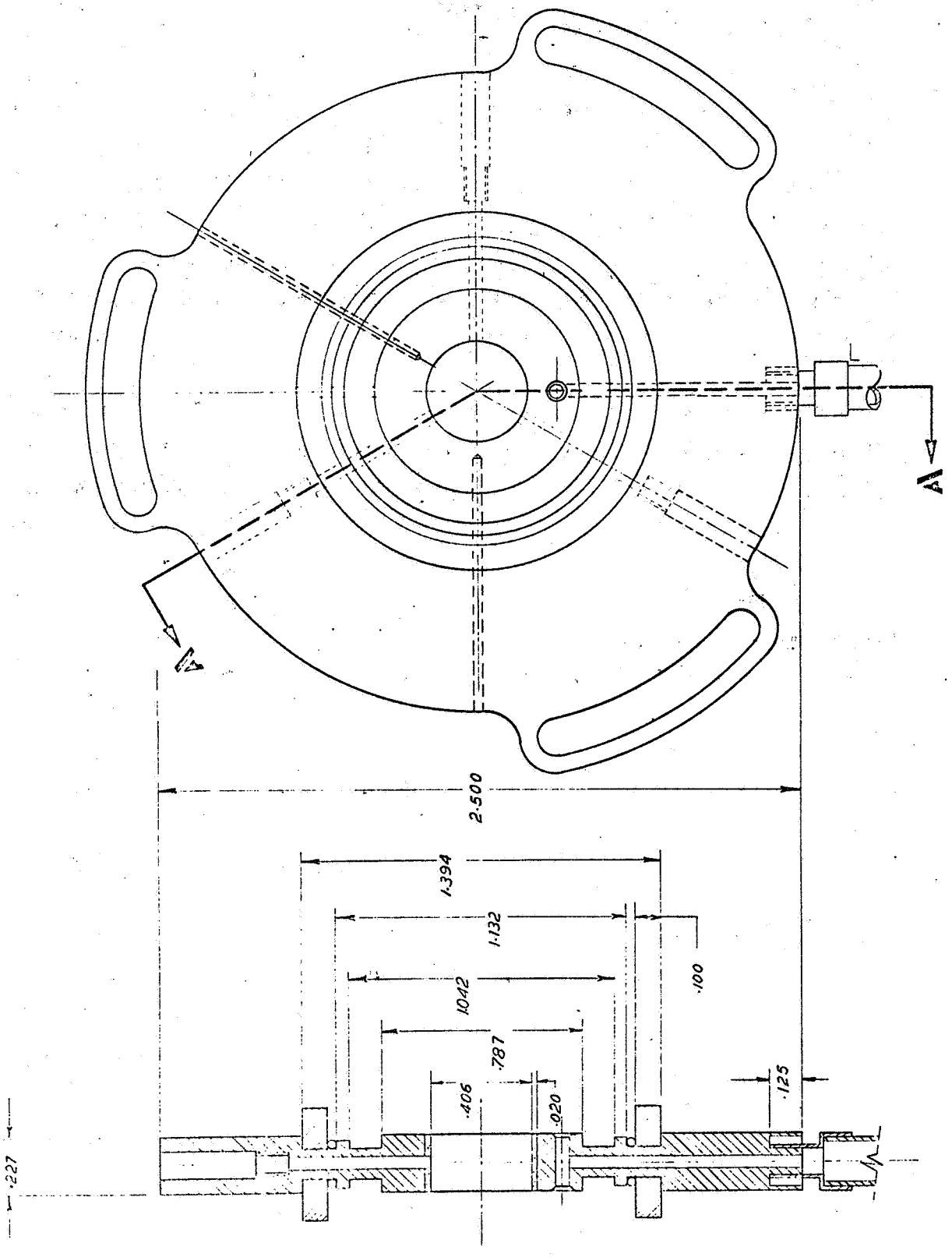

Figure 3-6. Collector, Radiator Assembly

where I is the drift current, φ_{coll} ($\varphi_{coll} \simeq 1.45$ for vapor deposited rhenium) is the collector work function, $\epsilon\ kT_{pl}/e$ is the random potential energy in the plasma. The value of ϵ is chosen as 1.3, and T_{pL} is selected to be 4000°K.

For: $I = 53$ amperes

$$Q_{el\ ht} \cong 108 \text{ watts}$$

The second term, Q_{rad}, is the net radiation heat transfer from emitter to collector.

$$Q_{rad} = \epsilon_{eff}\ \sigma A\ (T_{em}^4 - T^4\ coll)$$

where ϵ_{eff} is the effective emissivity of the electrode system. The net radiation heat transfer for $T_{em} = 1800°K$, $T_{coll} = 973°K$, $\epsilon_{eff} = 0.17$ and for an area of 2 cm^2 is:

$$Q_{rad} \simeq 17 \text{ watts}$$

The last term, $Q_{cs\ cond}$, cesium conduction is

$$Q_{cs\ cond} \approx 4.0 \text{ watts}$$

for a cesium temperature of 588°K.

The total collector heat load, Q_{total}, is

$$Q_{total} \cong 129 \text{ watts}$$

With the computed heat load of $\simeq 129$ watts, the average temperature of the radiator can be calculated using the dimensions of Fig. 3-6. Using the solution for a cylindrical plate of thickness, ℓ, with a hole in the center of radius, r_i, and the perimeter with radius, r_o, and a thermal heat flux, Q, the ΔT is expressed as

$$\Delta T = \frac{(\text{Ln } r_o - \text{Ln} r_i)\ Q}{K 2\pi \ell}$$

where K is the thermal conductivity of the material.

For a molybdenum collector thickness, ℓ, of 0.125 in., r_i = 0.56 cm and r_o = 1.9 cm, operating at a surface temperature of 993°K and 129 watts heat flux the temperature at the collector root (top of Rokide "C" portion in Fig. 3-5) is 917°K.

This yields a ΔT of 76° from collecting surface to the collector base. The ℓ chosen in the above calculation was the thickness of the smallest cross section (i.e., the area of the cutout for the niobium weld ring and the side wall spacing ceramic). However, if it is assumed that ℓ is 0.227 in., the collector-radiator ΔT from collecting surface to the collector base is 42°.

A radiator of $\approx$ 40 sq cm will reject the computed heat load of 129 thermal watts, when radiating at an average temperature of 910°K and an emissivity of 0.78 (Rokide "C").

3.1.4 PREFABRICATED METAL-TO-CERAMIC SEALS

The cylindrical converter has two seals which (1) electrically insulate the emitter from the collector, (2) provide structural support between the emitter and collector, and (3) provide a hermetic seal between the inside of the device and the ambient environment.

Figure 3-7 shows the prefabricated metal-to-ceramic seal assembly. The seal assembly is designed to operate reliably at $\approx$ 1000°K and the seal components contain materials that exhibit low vapor pressures at the temperature encountered during fabrication and operation.

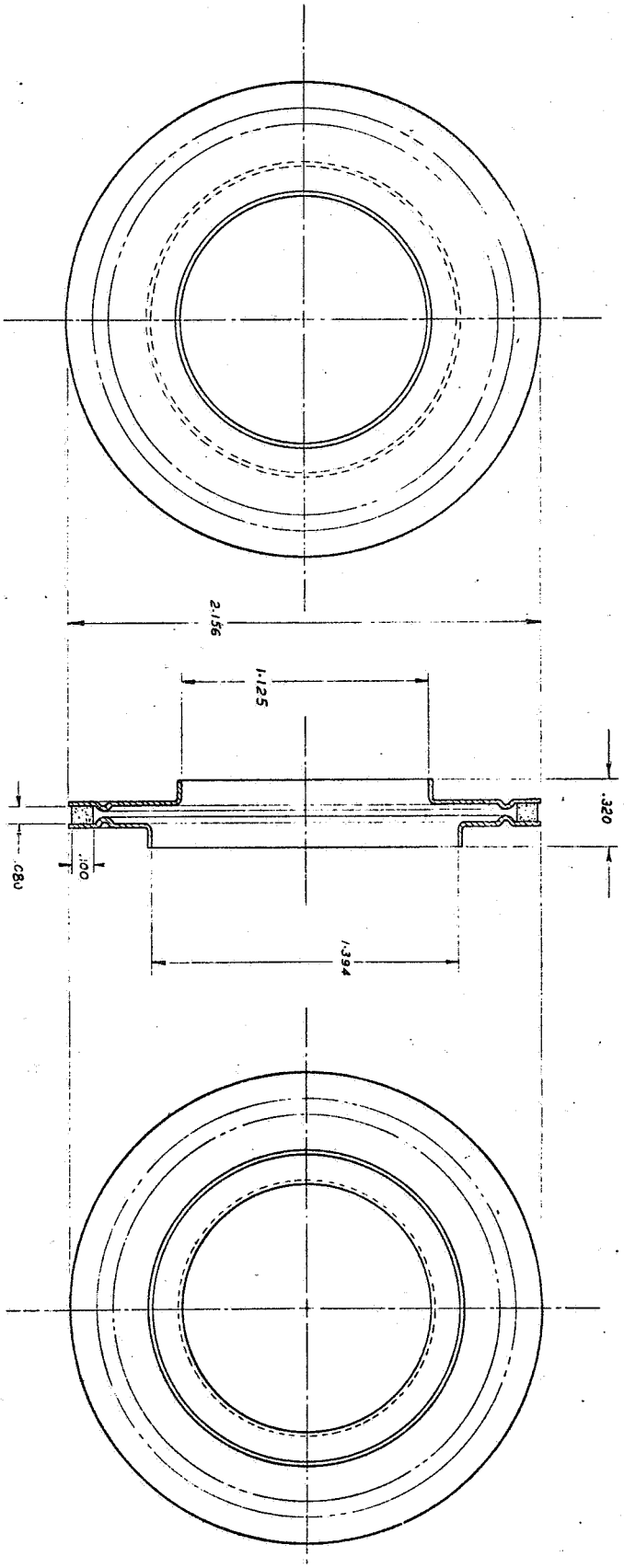

Figure 3-7. Seal Assembly, Prefabricated

The metal flanges are 0.020-in. niobium active alloy (Ni-Zr) brazed in vacuum to a high purity alumina insulator (AL995). The niobium flange is formed with a small convolution to allow for self fixturing of the Al_2O_3 insulator, while brazing.

Also, the niobium flanges contain right angle bends to allow for axial expansion of the converter during operation.

The prefabricated seals are electron beam welded to the emitter lead strap and the collector-radiator weld ring during final converter assembly.

3.1.5 CESIUM RESERVOIR

The cesium reservoir is thermally isolated from the radiator base by machining a thin wall section in the reservoir tubulation. A heater is titanium brazed to the reservoir to enable the cesium pressure in the converter to be adjusted.

The tantalum reservoir tubulation is electron beam welded as an assembly to a tantalum adapter which is titanium brazed in the collector radiator subassembly.

Thermal design calculations are obtained from consideration of heat transfer by conduction from the collector-radiator base to the reservoir and (for small radiation loss) is given by

$$Q = -KA\Delta T/\Delta X$$

where Q is the thermal conduction in watts, K is the thermal conductivity, and $\Delta T/\Delta X$ is difference in temperature per unit length in distance along the reservoir.

Assume that the collector-radiator is to be operated at 923°K and that the tantalum reservoir is to be maintained at 553°K. The tantalum tubulation has the dimensions of 0.187 in. outside diameter with a 0.007-in. wall for a length of 1 in.

The conduction heat transfer to a first approximation is:

$$Q = 0.16 \times 4.186 \times 0.024 \text{ cm}^2 \times \frac{370^\circ}{2.54}$$

$$Q = 2.3 \text{ watts}$$

This amount of heat can be rejected by a Rokide "C" coating ($\epsilon = 0.78$) on surface area of 6 cm^2 for 553°K operation.

3.2 THERMAL MOCKUPS

3.2.1 EMITTER ENVELOPE THERMAL MOCKUP

The side wall spacing in the cylindrical converter between the envelope wall and the collector assembly is $\approx$ 12 mils on a side. To determine whether the deflection of the heat choke (i.e., warpage or oil canning) due to thermal expansion, could be of sufficient magnitude to electrically short the envelope to the collector, a thermal mockup of the emitter was fabricated and tested. Figure 3-8 is a sketch of the emitter-envelope thermal mockup.

The thermal mockup dimensions correspond exactly to the converter emitter, emitter support structure, and emitter lead straps. Tantalum was selected as the structural material of the mockup because it has similar expansion characteristics to rhenium, it is inexpensive, and it is easily machined.

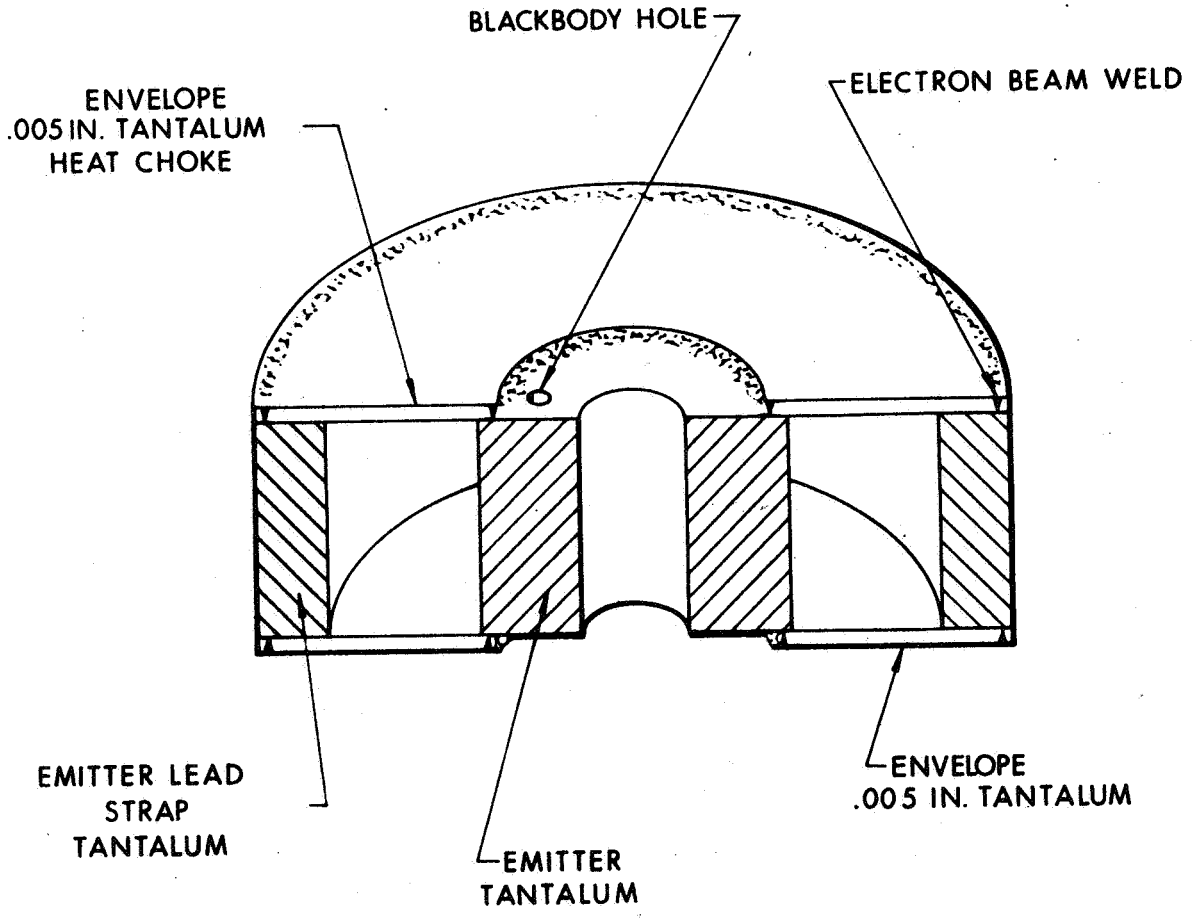

Figure 3-8. Emitter Heat Choked Envelope, Thermal Mockup

The center cylinder which simulated the emitter had a 10:1 blackbody hole for determining temperatures with a micro-optical pyrometer. The emitter support structure consisted of two flat annuli of 0.005 in. thick tantalum which were electron beam welded to the emitter and to an outer tantalum ring which simulated the emitter lead strap. The flatness of the emitter support structure (as welded) was measured and found to be flat to a total indicator reading (TIR) of 0.015 in. on both sides.

The emitter of the mockup was heated by an electron bombardment heater to 1800°K and the emitter lead strap portion was allowed to come to $\simeq$ 1050°K by heat sink strapping. Visual observations of the emitter envelope mockup while at temperature showed no gross warpage or oil canning, and the electron beam welds remained intact.

After a number of thermal cycles the unit was taken off test to measure the flatness of the envelope. The flatness of the heat choked envelope was again measured on two sides and found to be flat to a TIR of 0.013 inch and bowing outward on one side and flat to a TIR of 0.008 inch and bowing inward on the second side.

Although measurement of the thermal deflection warpage at temperature was not attempted, it is felt that the cold warpage indicated by the above measurement is enough to warrant sapphire rods placed between the heat choke envelope and the collector-radiator to ensure that the growth at temperature be forced in the outwards direction. However, since the integrity of the electron beam welds in the thermal mockup remained good, it is felt that this approach will most likely yield a reliable envelope design.

3.2.2 RADIATOR HEAT REJECTION

An integral molybdenum collector-radiator discussed in Subsection 3.1.3 was fabricated to provide a full-scale test for radiator heat rejection of the computed collector heat load of 129 watts.

Figure 3-9 shows the collector-radiator with thermocouple locations for measuring temperature. The radiating area is approximately 40-42 cm^2 on two sides with an emittance of 0.79 (Rokide "C"). The assembly was mounted in a vacuum system and heated indirectly at the collector surface by electron bombardment. Temperature profiles for four different collector temperatures were obtained and plotted (see Fig. 3-10).

The total heat load, Q_{total}, that the collector-radiator rejects is summed as follows:

$$Q_{total} = Q_{rad\ moly} + Q_{rad} + Q_{cond}$$

where $Q_{rad\ moly}$ is the heat rejected by radiation from the molybdenum collector portion, Q_{rad} is the heat rejected by radiation from the radiator (Rokide "C" portion), and Q_{cond} is the heat lost by conduction into the mounting straps.

The first term, $Q_{rad\ moly}$, is expressed by

$$Q_{rad\ moly} = A_{moly}\ \varepsilon\sigma T^4$$

where ε = emittance (molybdenum $\cong$ 0.1)
σ = Stefan Boltzmann constant = 5.66×10^{-12} watts cm^{-2} deg^{-4}
A = area of radiation (cm^2)
T = average temperature of molybdenum (^oK)

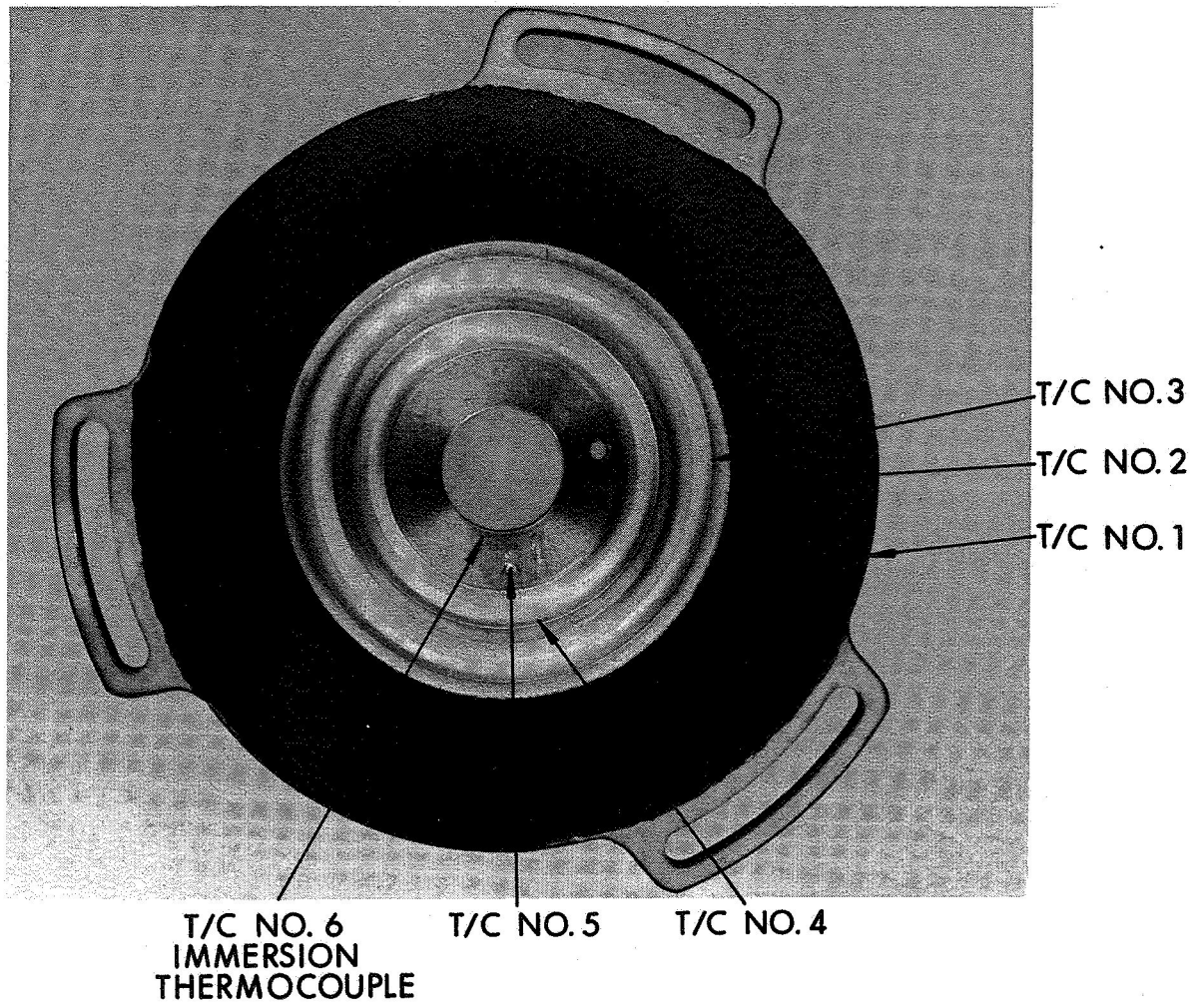

Figure 3-9. Collector-Radiator Thermal Mockup Showing Thermocouple Location for Measurement of Temperature to Determine Radiator Heat Rejection

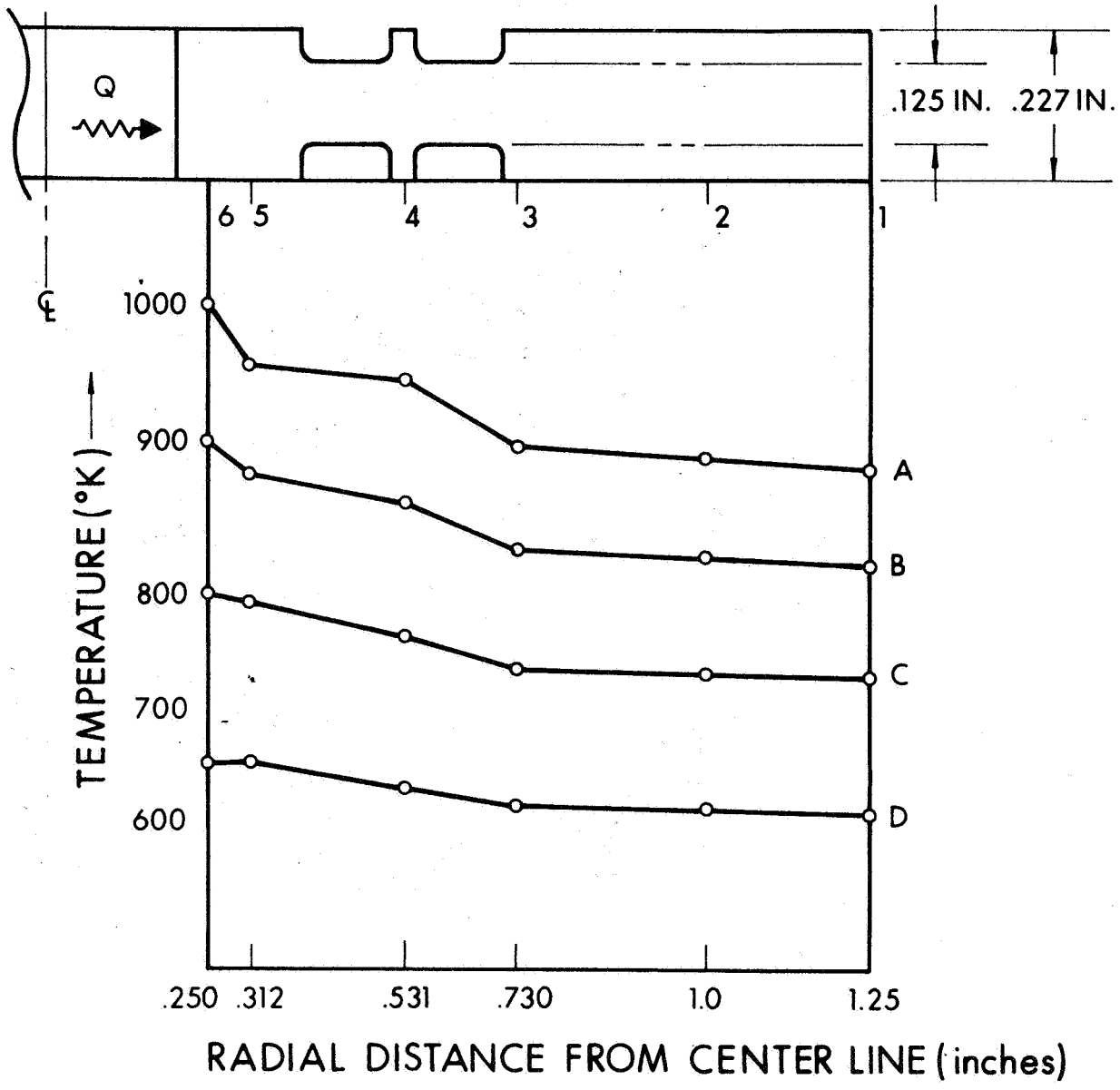

Figure 3-10. Radial Temperature Distribution of the Cylindrical Converter Collector-Radiator Assembly as a Function of Collector Temperature

The total area of the molybdenum collector (from the collecting surface to thermocouple No. 3) is 39 cm^2. From Fig. 3-10, curve "A," the average temperature is $\simeq 950^{\circ}K$, therefore

$$Q_{rad\ moly} \simeq 39\ cm^2 \times 0.49\ W/cm^2$$

$$Q_{rad\ moly} \simeq 19\ watts$$

The second term, Q_{rad}, is the heat rejected from the Rokide portion of the radiator. From curve A, the average temperature of the radiator is $910^{\circ}K$ (obtained for thermocouple No. 2). The area of the radiator is 42 cm^2. The emittance of this radiating section is 0.79 (Rokide "C"); therefore,

$$Q_{rad} = 42\ cm^2 \times \frac{3\ watts}{cm^2}$$

$$Q_{rad} = 126\ watts$$

The final term is the heat conducted down the mounting straps, Q_{cond}. It is estimated to be approximately 15-20 watts.

The total heat, Q_{total}, rejected from the collector-radiator is 160-165 thermal watts. Therefore, the collector-radiator design can accommodate the calculated heat load of 129 thermal watts discussed in Subsection 3.1.3 and in addition provide for the view factor correction when several collector-radiators are stacked in a generator configuration.

REFERENCES

1. Azizov, U. V., Vakhidov, U. V., Sulmanov, V. M., Sheinberg, B. N., Shuppe, G. N., Soviet Physics--Solid State, Vol. 7, No. 9, 2232, (1966)

2. Protopopov, O. D., Mikheeva, E. V., Sheinberg, B. N., Shuppe, G. N., Soviet Physics--Solid State, Vol. 8, No. 4, 909, (1966)

3. Savitskii, E. M., et al, Soviet Physics--Technical Physics, Vol. II, No. 7, 974, (1967)

4. R. Wichner and T. H. Pigford, Thermionic Conv. Spec. Conf., Houston (1966)

5. A. Campbell and D. Jacobson, Thermionic Research and Development Program, Final Report, Contract NAS7-514, EOS 7118-Final (1968)